

See discussions, stats, and author profiles for this publication at: <https://www.researchgate.net/publication/266383335>

Identification of novel PTP1B inhibitors by pharmacophore based virtual screening, scaffold hopping and docking

ARTICLE in EUROPEAN JOURNAL OF MEDICINAL CHEMISTRY · OCTOBER 2014

Impact Factor: 3.45 · DOI: 10.1016/j.ejmech.2014.09.097

READS

248

17 AUTHORS, INCLUDING:



Vishal M. Balaramnavar

Central Drug Research Institute

24 PUBLICATIONS 75 CITATIONS

[SEE PROFILE](#)



Arun Rawat

Central Drug Research Institute

15 PUBLICATIONS 35 CITATIONS

[SEE PROFILE](#)



Santosh Kumar

Rajendra Agricultural University

67 PUBLICATIONS 210 CITATIONS

[SEE PROFILE](#)



Swayam Prakash Srivastava

Kanazawa Medical University

28 PUBLICATIONS 218 CITATIONS

[SEE PROFILE](#)



Original article

Identification of novel PTP1B inhibitors by pharmacophore based virtual screening, scaffold hopping and docking



Vishal M. Balaramnavar ^{a,1}, Rohit Srivastava ^{b,1}, Neha Rahuja ^b, Swati Gupta ^a, Arun K. Rawat ^b, Salil Varshney ^c, Hardik Chandrasana ^d, Yashpal S. Chhonker ^d, Pawan Kumar Doharey ^b, Santosh Kumar ^a, Sudeep Gautam ^b, Swayam Prakash Srivastava ^b, Rabi Sankar Bhatta ^d, Jitendra Kumar Saxena ^b, Anil Nilkanth Gaikwad ^c, Arvind K. Srivastava ^b, Anil K. Saxena ^{a,*}

^a Division of Medicinal and Process Chemistry, CSIR-Central Drug Research Institute, Jankipuram Extension, Lucknow 226021, UP, India

^b Division of Biochemistry, Central Drug Research Institute, CSIR, Jankipuram Extension, Lucknow 226021, UP, India

^c Division of Pharmacology, CSIR-Central Drug Research Institute, Jankipuram Extension, Lucknow 226021, UP, India

^d Pharmacokinetics and Metabolism Division, CSIR-Central Drug Research Institute, Jankipuram Extension, Lucknow 226021, UP, India

ARTICLE INFO

Article history:

Received 1 May 2014

Received in revised form

3 September 2014

Accepted 30 September 2014

Available online 2 October 2014

Keywords:

PTP1B inhibitors

Pharmacophore modeling

Scaffold hopping

Docking

Synthesis and biological activity

ABSTRACT

Design and synthesis of protein tyrosine phosphatases-1B (PTP1B) inhibitors are important for the drugs targeted to treat diabetes and obesity. The pharmacophore modeling, docking and scaffold hopping techniques have been applied to discover the novel PTP1B inhibitors. The ten prioritized compounds (**115–119, 120–121, 127, 130–131**) from the library of 86 compounds were synthesized and found positive in the micro molar range for PTP1B in-vitro inhibitory assays as compared to Suramin (IC_{50} 9.5 μ M). Among these five active compounds (**115–119**) were tested in STZ-s induced diabetic rat model and the most active compound **115** in this test, was further tested in C57BL/KsJ-db/db mice where it significantly improved OGTT along with the fasting and random blood glucose level. The treatment by the compound **115** significantly improved the insulin resistance and insulin signaling by restoring the insulin level and normalizing the serum lipid profile. Compound **115** also augmented the insulin action by modulating the expression of genes involved in insulin signaling like IRS 1–2, PI3K, PTPN1, Akt2, AMPK and PPAR- α . Western blot analysis of both skeletal muscle and liver demonstrated that proteins and intermediate enzymes of insulin signaling were also increased as compared to control group. The compound **115** was also investigated for anti-adipogenic effect on 3T3L-1 cells. The compound **115** inhibited MDI induced lipid accumulation in a dose-dependent manner. The oral bioavailability of compound **115** was ~10.29% after 30 mg/kg oral dosing assessed in rat.

© 2014 Elsevier Masson SAS. All rights reserved.

1. Introduction

Protein tyrosine phosphatases (PTPs) belong to a large family of signaling enzymes and serve as paramount regulatory components in numerous cell functions, including growth, mitogenesis, motility, cell–cell interaction, metabolism, gene transcription, and immune response [1–3]. The unregulated levels of these enzymes have been

observed in the diabetes, obesity and osteoporosis [1–8]. The two types of the enzymes present in the cellular environment as protein tyrosine kinases (PTKs) catalyze the phosphorylation of phosphotyrosine residues of proteins. The protein tyrosine phosphatase (PTP) which catalyzes the dephosphorylation of phosphotyrosine residues on proteins, while the PTP1B dephosphorylates the activated insulin receptor and thus inhibits specific protein-to-protein association involved in the deactivation of the downstream signaling proteins [5]. It consequently results in the hyperglycemia due to a reduction of the metabolic activity of insulin [9–11]. Recent studies in knockout mouse models have provided evidences that strongly implicate PTP1B as a specific regulator of the insulin action pathway with its influence in the body weight regulation and energy expenditure. Apparently in healthy phenotype, the PTP1B

Abbreviations: PTP1B, protein tyrosine phosphatase-1B; QSAR, quantitative structure activity relationship; PBVS, pharmacophore based virtual screening; SAR, structure–activity relationship; HSA, human serum albumin.

* Corresponding author.

E-mail address: anilsak@gmail.com (A.K. Saxena).

¹ These authors have contributed equally.

knockout strain exhibited lower fasting insulin and glucose levels while keeping the other alterations consistent with enhanced insulin sensitivity, including an accentuated drop in blood glucose during insulin tolerance testing.

Type-2 diabetes mellitus is characterized by unresponsive peripheral tissues to insulin or the pancreatic impairment to secrete the insulin or both. The insulin resistance seems to be the common link between the two diseases viz. obesity and diabetes. The insulin resistance in the type 2 diabetes is due to post receptor signal transduction defects. The inter conversion of proteins between the phosphorylated and non-phosphorylated forms is one of the most prevalent mechanisms for the reversible modulation of enzymes [4]. Thus, the inhibition of PTP1B resulted in the induction of the sensitivities of insulin and leptin and showed the protective effect on diet induced obesity in mice [12–14]. The recently reported studies in the knockout PTP1B mice showed improved insulin sensitivity and confrontation to obesity [12,13,15–20]. Thus supporting the PTP1B as an important target for the treatment of diabetes and obesity. Therefore design and development of PTP1B inhibitors was undertaken as an important therapeutic strategy in the search of oral antidiabetic and antiobesity related drugs.

The wealth of information is available for the human PTP1B co-crystal structures with the bound inhibitor to distinguish the structural features essential for its binding. The binding site of the PTP1B generally consisted of amino acids viz. His–Cys–Ser–Ala–Gly–Ile–Gly–Arg which are involved in binding to phosphorylated tyrosine moiety of the substrate proteins [18,21]. Many peptidic and non-peptidic molecules binding with the known active site as well as to the adjacent binding site are reported [17,18,22–26]. The binding sites are divided into (A, B, C) according to impact on different ligand's binding to these regions A site (primary phosphate-binding pocket) is the most polar region of the protein and contains the catalytic site where phosphate ions interact with the signature motif; B site is the secondary phosphate-binding pocket that plays a role in substrate specificity; C site is a large flat region that can accommodate negatively charged substituents [27].

Recently, a number of synthetic PTP1B inhibitors with sub-micro molar or nanomolar activities have been discovered through high-throughput screening and structure-based design [28,29]. These compounds although have great potential but suffer from the limitation of the low cell permeability and low bioavailability which hinder their development as effective candidate drugs [30,31]. The major reason behind this is the presence of highly negatively charged residues (including difluoromethylphosphonates, carboxymethylsalicylic acids, and oxalyl amino benzoic acids) which mimic the phosphate group in IRS [28,29]. Additionally, owing to the structural homology throughout many families of PTPs, it is challenging to identify selective inhibitors specific to each PTP. Therefore, although there are a number of patents, molecules under phase I clinical trials and research articles available in the past for this target still there is an urgent need for the design and development of therapeutically useful and orally bioavailable PTP1B inhibitors [32–35].

The drug discovery approaches including advanced structure activity relationship studies in the last few decades have facilitated the design of many NCEs in the diverse classes of diseases viz. Alzheimer's disease (AD), Cancer, Diabetes [36–40]. The ligand based modeling is possible by using SYBYL/comparative molecular field analysis (CoMFA) [41] and comparative molecular similarity indices analysis (CoMSIA) [42]; Catalyst/HypoGen and HipHop [43]. Among these CoMFA, CoMSIA and structure based approaches were reported for PTP1B as a target for diabetes [44–47]. There are few limitations of both these approaches. The pharmacophore based virtual screening methods are found superior than both the CoMFA,

CoMSIA and structure-based methods in their ability to screen very large databases faster for retrieving more structurally diverse leads than protein ligand docking [48–50]. The development of the catalyst derived pharmacophore models has been very useful in virtual screening of chemical libraries [36,40]. Among the two approaches HipHop and HypoGen of the catalyst software, the latter is more reliable than former because it is based on the quantitative measures of biological activities with at least 3–4 orders of difference while in former, the requirement is a small set of known active molecules [51,52].

In view of the above limitations of structure and ligand based approaches we have devised a hybrid approach capitalizing on the mutual strengths of both of the approaches and compensating their limitations. This hybrid approach utilizing the pharmacophore based virtual screening (PBVS), scaffold hopping for focused library design, followed by docking based virtual screening (DBVS) has been recently applied in the discovery of NCEs for Alzheimer's disease reported by our group [40]. In continuation of our work on PTP1B inhibitors, in the present article we have utilized this hybrid approach in designing and synthesizing the NCEs as PTP1B inhibitors where ten identified and prioritized leads have been synthesized and evaluated as promising PTP1B inhibitors as anti-diabetic agents. The pharmacokinetic properties of drug molecules in humans are strongly governed by their reversible or irreversible binding with human serum albumin (HSA) [53–55]. Since BSA is a 66 kDa monomer protein having 80% structural homology with human serum albumin (HSA) [56–58], the bovine and human serum albumin exhibit similar binding. Considering the low cost and easy availability of BSA over HAS [59], the BSA binding studies of the promising molecules have been carried out. In order to further validate these BSA binding studies, oral bioavailability of these molecules was also carried out and the results of these studies are presented in this manuscript.

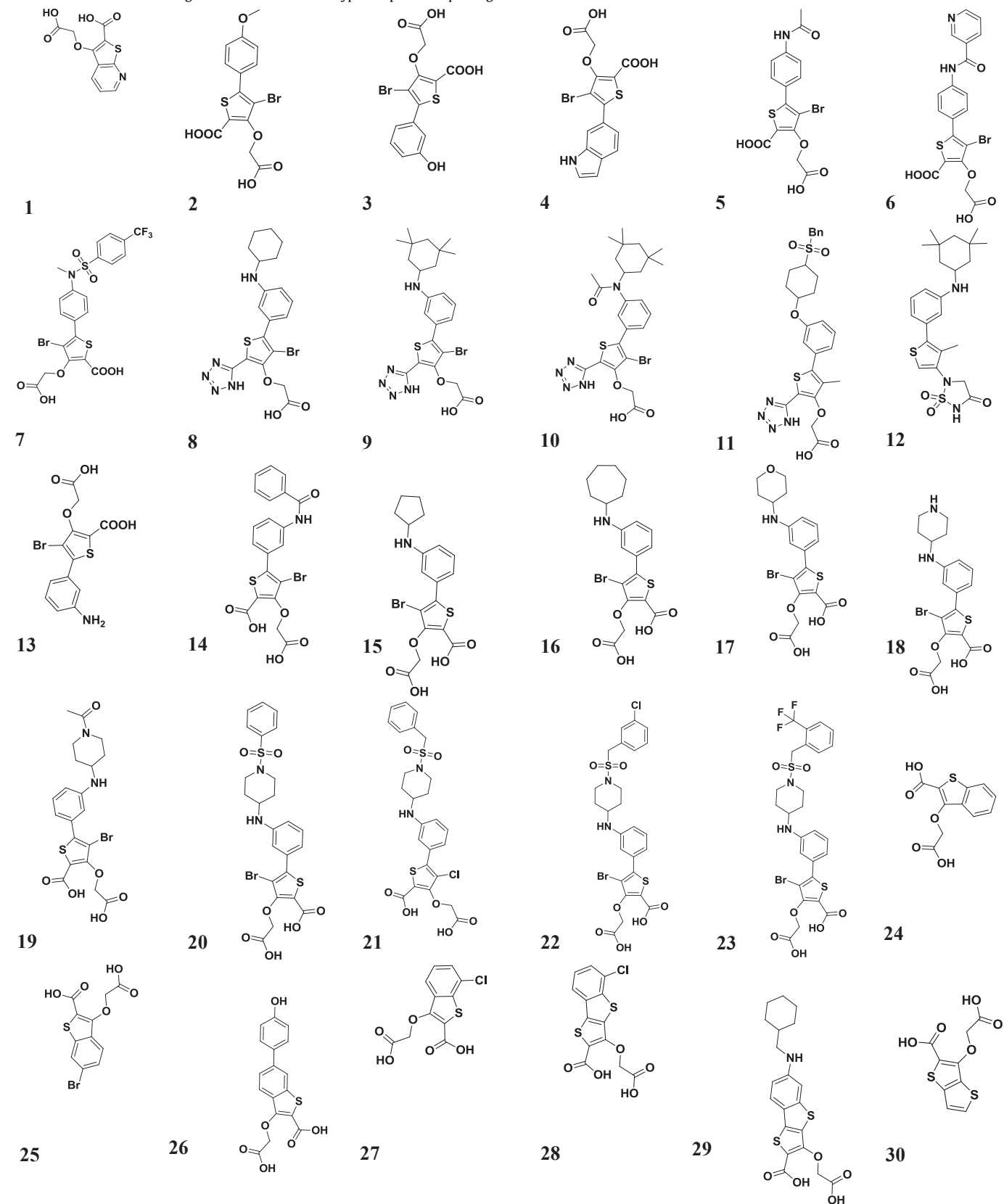
2. Results and discussion

2.1. Generation and selection of pharmacophore models

The 3D QSAR pharmacophore model generation protocol using 30 training set molecules (Table 1) resulted in the development of ten pharmacophore models comprised of four features viz. Hydrophobic Feature (H), A: H-Bond Acceptor Feature; NI: Negatively Ionizable Group; Ring Aromatic (R) (Fig. 1). The null and the fixed costs among the pharmacophore hypothesis were 215.795 and 118.723 respectively. The greater difference 97.072 than the stipulated value of 70 between the fixed and the null cost indicate good robustness of the models. The difference between the null and total cost for the best model was 85.296 indicating its more than 90% reliability with a true correlation of the data (Table 2). The configuration cost in the best hypothesis was 16.6903 and for all the hypotheses was lesser than 17 corresponding to $2^{16.6903}$ hypotheses. A value >17 indicates that correlation for any generated pharmacophore is most likely due to chance correlation since Catalyst cannot consider more than 2^{17} hypotheses in the optimization phase and so the rest are left out. According to above criteria's the total cost of the good pharmacophore model should be close to the fixed cost and distant from the null cost i.e. the model so developed is an excellent model. The correlation coefficient (*r*) values of 10 pharmacophore models ranged between 0.947 and 0.939 (Table 2) suggesting that all the 10 models are capable of predicting the PTP1B inhibitors IC₅₀. Besides this the best pharmacophore model (Hypo-1) with the structural features 2H, 1A, 1NI, 1R had lowest error (112.66), lowest RMSD 0.885 (<1.5), and showed the highest fit value 9.51 for the most and 3.81 for the least active compounds respectively. This pharmacophore model with high predictability is described along

Table 1

The Structures of all 30 training set molecules used for HypoGen pharmacophore generation.



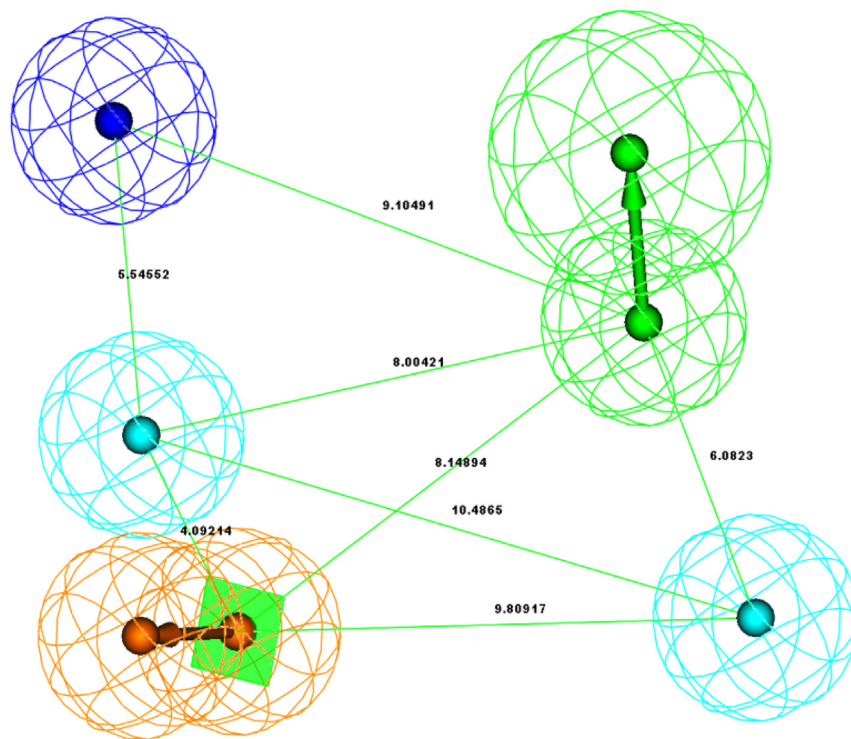


Fig. 1. The best pharmacophore model Hypo-1 with distance constraints. The important features extracted from training set of **30** compounds using Discovery studio with its interfeature distances. The features are color coded as follows: green: HBA; and cyan: HY; Orange: ring aromatic. (For interpretation of the references to colour in this figure legend, the reader is referred to the web version of this article.)

with interfeature distances in Å in Fig. 1. It predicted the training set compounds very accurately (Table 3) with considerably low rms error and thus correctly categorized them into highly (+++), moderately (++) and inactive (+) classes. The error cost in the Hypo-1 is less than 10 indicating that the difference in the estimated K_i values and the experimental K_i values is less than one order of magnitude. The mapping of the most active compound **21** from the series revealed that all the features were mapped to the pharmacophore model with least displacement from the centroid (Fig. 2A). The benzene ring from the 1-benzylsulfonyl piperidin-4-ylamino group and the 4-chloro substitution of 4-chlorothiophene-2-carboxylic acid mapped with the two hydrophobe (H) functions of Hypo-1, while one oxygen atom from $-\text{SO}_2$ group from 1-benzylsulfonyl substitution from piperidin group mapped well

with one hydrogen bond acceptor (A) function. The 5-amino phenyl substitution of the compound **21** mapped to the ring aromatic (R) function of the Hypo-1. The 3-carboxymethoxy group of the compound **21** mapped well to the one negative ionizable (NI) function of the Hypo-1. The least active compound **30** (Fig. 2B) mapped only two features one hydrophobe (H) and one negative ionizable (NI) while missed three features viz. one hydrogen bond acceptor (A), a hydrophobe (H) and one ring aromatic feature (RA).

2.2. Pharmacophore validation

In order to validate Hypo-1, which had high statistical significance in terms of correlation, cost-function quality, and ability to explain the training set compounds, an additional validation of the

Table 2
Summary of Top 10 Pharmacophore Models obtained from Catalyst/HypoGen Run.

Hypo. ^a	TC ^b	NC-TC ^c	EC ^d	rmsd ^e	r ^f	Features ^g	Config ^h	Ex.V. ⁱ
1	130.499	85.296	112.66	0.885	0.947	2H, 1A, 1NI, 1R	16.6903	0
2	130.963	84.832	112.17	0.866	0.950	1H, 1A, 1NI, 1R	16.6903	0
3	131.426	84.369	112.919	0.895	0.946	1H, 1A, 1NI, 1R	16.6903	0
4	131.694	84.101	113.057	0.899	0.945	1H, 1A, 1NI, 1R	16.6903	0
5	132.059	83.736	113.558	0.918	0.943	1H, 1A, 1NI, 1R	16.6903	0
6	132.429	83.366	113.776	0.943	0.942	1H, 1A, 1NI, 1R	16.6903	0
7	132.494	83.301	114.678	0.938	0.938	1H, 1A, 1NI, 1R	16.6903	0
8	132.537	83.258	114.717	0.938	0.937	1H, 1A, 1NI, 1R	16.6903	0
9	133.053	82.742	114.883	0.965	0.937	1H, 1A, 1NI, 1R	16.6903	0
10	133.135	82.660	114.499	0.952	0.939	1H, 1A, 1NI, 1R	16.6903	0

^a Hypo.: Hypothesis number in ascending order of Total Cost.

^b TC: total cost.

^c NC-TC: Null Cost (215.795)-total cost (130.499) or cost difference means the difference between null cost and total cost.

^d EC: error cost.

^e rmsd: root mean square deviation.

^f Correlation coefficient.

^g Abbreviations used for features H: Hydrophobic Feature; A: HBA-Bond Acceptor Feature; NI: Negatively Ionizable Group; R: Ring Aromatic Group.

^h Config.: Configuration Cost.

ⁱ Ex.V.Number of Excluded Volumes. Fixed Cost (118.723).

Table 3

Experimental and Predicted K_i (μM) Values of the 30 training set compounds based on the pharmacophore model Hypo-1.

Comp. No.	Fit value	K_i (μM)		Error	Activity scale ^c	
		Est. Act ^a	Obsd. act. ^b		Est. scale	Obsd. scale
1	3.93	130	230	-1.7	+	+
2	5.76	1.8	3	-1.6	+++	+++
3	5.75	1.9	1	1.9	+++	+++
4	5.78	1.8	0.57	3.1	+++	+++
5	5.78	1.8	0.5	3.6	+++	+++
6	5.84	1.5	0.82	1.9	+++	+++
7	6.51	0.33	1.2	-3.6	+++	+++
8	5.76	1.8	18	-9.8	++	++
9	5.78	1.8	1.6	1.1	+++	+++
10	6.03	0.99	4.6	-4.6	++	++
11	7.11	0.083	0.3	-3.6	+++	+++
12	5.14	7.7	15	-2	++	++
24	4.01	100	160	-1.5	++	++
30	3.87	140	280	-1.9	+	+
25	3.91	130	42	3.1	++	++
26	4.57	29	26	1.1	++	++
27	4.15	76	120	-1.6	++	++
28	4.71	21	10	2.1	++	++
29	5.74	1.9	0.68	2.8	+++	+++
13	5.75	1.9	1.7	1.1	+++	+++
14	5.78	1.8	2.1	-1.2	+++	+++
15	5.76	1.9	0.39	4.8	+++	+++
16	6.24	0.62	0.12	5.2	+++	+++
17	6.64	0.25	0.31	-1.3	+++	+++
18	5.75	1.9	3.8	-2	++	++
19	6.8	0.17	0.19	-1.1	+++	+++
20	7.52	0.032	0.055	-1.7	+++	+++
21	9.15	0.00076	0.00068	1.1	+++	+++
22	8.25	0.0061	0.01	-1.6	+++	+++
23	7.54	0.031	0.006	5.2	+++	+++

^a Est = estimated.

^b Obsd = observed.

^c Activity scale: +++(K_i 0.00068 μM –3 μM), ++(K_i 3.8 μM –160 μM moderately active), +(K_i 230 μM –280 μM , poorly active).

pharmacophore model was carried out by using **82** compounds retained in the test set to estimate the predictability of this model. As expected, the Hypo-1 explained well the activity variation among the test set compounds with the good correlation coefficient value ($r = 0.842$). The **82** compounds were classified assuming their activity as highly active 0.00068 μM –3 μM (+++), moderately active 3.8 μM –160 μM (++) and least active 230 μM –280 μM (+) (Table 4) except compounds **36**, **37**, **40**, **53** and **69** which

belonged to the highly active class but predicted as moderately active. The structures of these compounds along with the reported activities in μM are presented in the supporting information (Supporting information, Table S1, page S3–S7). This pharmacophore model Hypo-1 was also validated by predicting the some PTP1B inhibitors under clinical trials and the most active compounds of some classes from literature (Reference 1–8, Supporting information, page S40–S42). The Hypo-1 predicted most of these compounds very well. The pharmacophore alignments of these compounds used as an external test set along with their fit values compared to predicted and reported K_i values are presented in the supporting information (Supporting information, Fig. S1, page S8). These studies further authenticated the validity of this pharmacophore model and added assertion of its applicability in virtual screening experiments for identification of NCE's as PTP1B inhibitors.

2.3. Pharmacophore complementarities in active site

In order to validate the complementarities of the pharmacophore model within the PTP1B binding site, the most active compound **21** from the dataset was docked to study the binding mode of the ligand in the PTP1B active site. Among the known co-crystallized structures of PTP1B inhibitors available in the RCSB Protein Data Bank (www.rcsb.org), the one,

co-crystallized with ligand BPPM (PDB ID 1AAX) was selected for docking studies [60]. The docking analysis revealed the most remarkable features of the PTP1B inhibitors in active site i) the hydrophobic and “ π – π ” stacking interactions with the Phe-182 (Fig. 3). ii) Strong hydrogen bond interactions with the side chain of Tyr-46 via “ π – π ” stacking, and hydrophobic interactions with Gly-259, Ser-216, Arg-24, Tyr-20. The ring aromatic (R) function of the pharmacophore model is well supported by the hydrophobic and “ π – π ” stacking interactions of the aromatic ring with Glu-115 and Lys-116. The one hydrogen bond acceptor (A) function of the pharmacophore model is also validated by the interactions of $-\text{SO}_2$ group with the Trp-179 and Pro-180. While the one negative ionizable function is validated by the interaction of 3-carboxymethoxy group with Arg-14.

2.4. Scaffold hopping

The process of searching the novel compounds with similar bioactivity to the reference compounds with different molecular

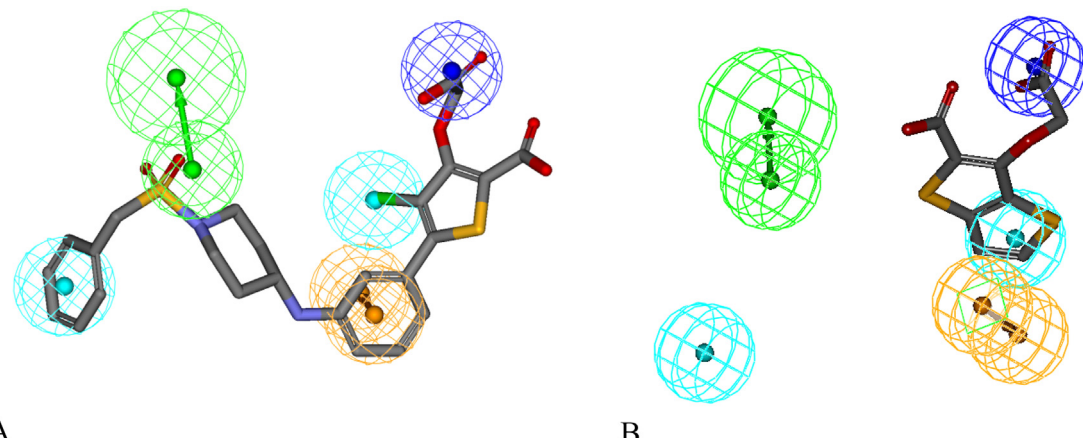


Fig. 2. Mapping of most active and least active compounds from training set. (A) The compound **21** in the training was predicted correctly as a most active compound because it maps all the features well and compound **30** was predicted correctly as LA. (B) Features are colored as hydrogen bond acceptor-green, cyan-hydrophobe, blue-negatively ionizable and orange ring aromatic.

Table 4Experimental and predicted K_i values of the **82** test set compounds based on the pharmacophore model Hypo 1.

Comp. No.	Est. Act. (μM)	Obs. Act. (μM)	Fit value	Predicted scale ^a	Exp. scale	Compound no.	Est. Act. (μM)	Obs. Act. (μM)	Fit value	Predicted scale	Exp. scale
31	71.69	160	4.17	++	++	54	64.3	120	5.02	++	++
32	29.65	18	4.55	++	++	55	0.0	1.3	7.37	+++	+++
33	1.82	3.2	5.77	+++	++	56	32.2	18	3.87	++	++
34	1.78	1.4	5.78	+++	+++	57	41.6	41	3.87	++	++
35	1.77	4	5.78	+++	++	58	34.7	16	3.878	++	++
36	1.80	3.3	5.77	+++	++	59	14.4	12	4.87	++	++
37	1.87	5	5.75	+++	++	60	14.0	14	4.88	++	++
38	1.89	0.3	5.75	+++	+++	61	1.7	1.7	5.78	+++	+++
39	1.86	1.6	5.76	+++	+++	62	0.4	4.3	6.46	+++	++
40	1.72	9	5.79	+++	++	63	62.8	16	3.88	++	++
41	1.78	0.62	5.78	+++	+++	64	74.4	77	4.16	++	++
42	1.72	0.6	5.79	+++	+++	65	87.5	61	4.08	++	++
43	1.52	2.5	5.84	+++	+++	66	87.2	52	4.08	++	++
44	0.82	0.74	6.11	+++	+++	67	50.2	128	4.55	++	++
45	1.71	0.2	5.79	+++	+++	68	25.2	30	4.63	++	++
46	1.77	1	5.78	+++	+++	69	1.7	20	5.79	+++	++
47	1.73	0.36	5.79	+++	+++	70	23.0	37	4.67	++	++
48	1.90	0.25	5.75	+++	+++	71	120.3	280	4.73	++	++
49	1.79	0.14	5.77	+++	+++	72	22.6	9.2	4.67	++	++
50	0.01	0.005	7.97	+++	+++	73	24.1	3.5	4.65	++	++
51	0.04	0.024	7.46	+++	+++	74	3.6	0.92	5.47	+++	+++
52	1.74	20	5.78	+++	++	75	19.7	1.7	4.74	+++	+++
53	81.32	170	5.77	+++	++	76	5.0	0.74	5.33	+++	+++
77	24.07	2.4	4.65	+++	+++	95	0.022	0.008	7.68	+++	+++
78	6.71	1.6	5.2	+++	+++	96	0.037	0.024	7.46	+++	+++
79	0.26	0.37	6.6	+++	+++	97	0.033	0.074	7.5	+++	+++
80	0.91	4	6.07	+++	+++	98	0.083	0.31	7.11	+++	+++
81	1.88	2	5.75	+++	+++	99	0.214	0.007	6.69	+++	+++
82	0.17	2.1	6.81	+++	+++	100	0.222	0.013	6.68	+++	+++
83	1.87	2	5.75	+++	+++	101	0.001	0.038	9.23	+++	+++
84	0.45	0.44	6.37	+++	+++	102	0.003	0.005	8.52	+++	+++
85	1.89	0.47	5.75	+++	+++	103	0.035	0.004	7.49	+++	+++
86	1.74	0.68	5.78	+++	+++	104	0.020	0.006	7.72	+++	+++
87	1.77	0.2	5.78	+++	+++	105	0.031	0.002	7.53	+++	+++
88	1.82	0.21	5.77	+++	+++	106	0.006	0.002	8.26	+++	+++
89	1.77	0.036	5.78	+++	+++	107	0.033	0.014	7.51	+++	+++
90	0.09	0.39	7.06	+++	+++	108	0.001	0.001	9.21	+++	+++
91	0.26	0.3	6.61	+++	+++	109	0.471	0.004	6.35	+++	+++
92	0.14	0.044	6.88	+++	+++	110	0.198	0.003	6.73	+++	+++
93	0.01	0.004	7.97	+++	+++	111	0.253	0.003	6.62	+++	+++
94	0.05	2	7.29	+++	+++	112	0.119	0.003	6.95	+++	+++

^a Activity scale: +++(K_i 0.00068 μM – 3 μM), ++(K_i 3.8 μM –160 μM moderately active), +(K_i 230 μM –280 μM , poorly active).

framework has been named as “scaffold hopping”. In the present study we applied our state of the art in drug design of NCEs using scaffold hopping technique. The best way to gain an insight into the possible scaffold is based on the structures of the reported clinically effective inhibitors/drugs, which has either reached in the market or had shown some success in the clinical trial phases. The common scaffold analysis of the clinically active compounds of PTP1B inhibitor class led us to design the scaffold with substituted N-benzyl-N-(2-hydroxy-2-phenylethyl) benzenesulfonamide (colored pink and turquoise in Fig. 4) substructure as a novel scaffold for the design of the focused virtual library. The strategy used for scaffold hopping is outlined in Fig. 4. In continuation of pharmacophore modeling the scaffold hopping protocol was also implemented for the identification of probable NCE's for this target. In view of this the two scaffolds with the targeted activity reported in the literature were used as template molecules for the scaffold hopping [61,62]. Both the scaffolds were used as substructures for constructing the new prototype using the substructural or medicinal chemical hybridization approach keeping in view the easy synthetic feasibility of the designed molecules (Fig. 4) [63]. The replacement of NC=O substructure from the core **B** of the structure **114a** by CH–OH in the new prototype represented by molecules (**115–119, 120–121, 127, 130–131**, Table 5) was based on the bioisosterism observed between them in our earlier work [64,65]. Based on this a focused virtual

library of **86** compounds was designed for virtual screening (Supporting information, Table S2 page S9, along with their predicted activity in Table S3, page S13).

2.5. Pharmacophore-based virtual screening

The PBVS has been well-accepted protocol for in-silico high-throughput screening process for the identification and optimization of novel lead molecules. The construction of the pharmacophore model was carried out on pTyr mimetics acting on catalytic site. These compounds were selected as they have shown good in-vitro PTP1B inhibitory activity but suffer from the limitation of the low cell permeability and low bioavailability which has hindered their development as effective candidate drugs [28,29]. The major reason behind this has been the presence of highly negatively charged residues (including difluoromethylphospho-nates, carboxymethylsalicylic acids, and oxalyl amino benzoic acids) which mimic the phosphate group in IRS [30,31] and thus prevent their action in vivo. In view of this the major task was to design the molecules lacking these functions and yet may provide electron rich site for interaction with Arg-221. Hence we designed the molecules which do have all other features of the developed pharmacophore except the highly negatively charged residues but in addition an electron rich –OH group to provide interaction with Arg-221.

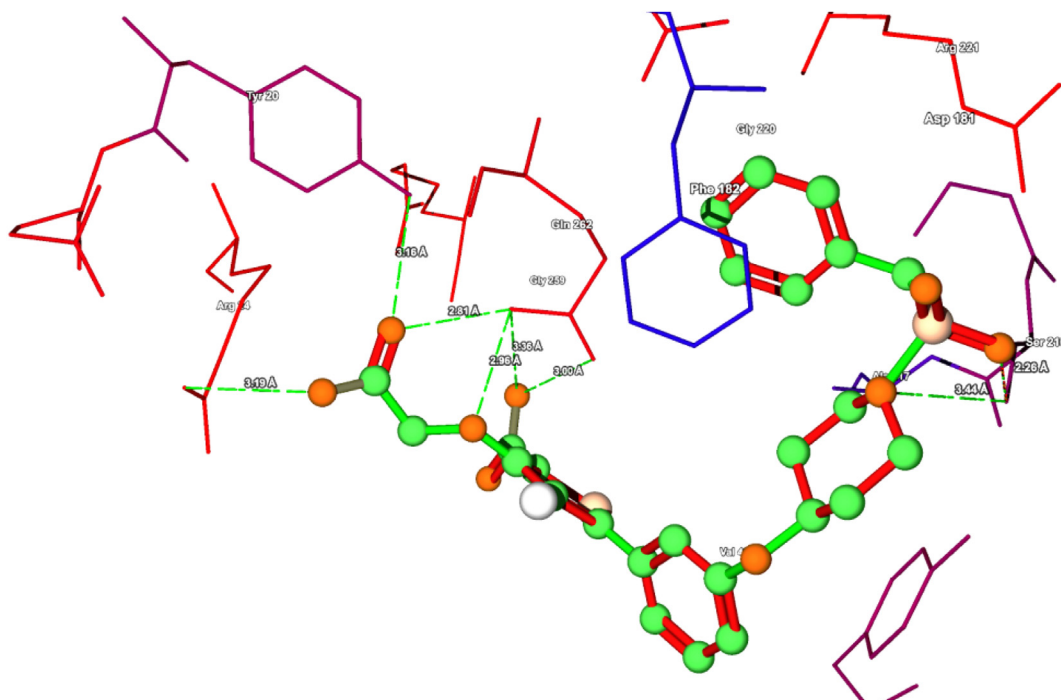


Fig. 3. The binding of the MA compound **21** from the dataset in the active site. The binding orientation was taken from the Molegro virtual docker. The receptors colored by hydrophobicity the red color indicates the hydrophilic interactions and the blue indicated the hydrophobic interactions and the ligand was colored by type of hydrogen bonding interactions. (For interpretation of the references to colour in this figure legend, the reader is referred to the web version of this article.)

Based on this strategy a focused virtual library of the potential PTP1B inhibitors were designed and mapped on to the best pharmacophore model Hypo-1 using the multiconformer generation protocol. It resulted in the identification of top **20** out of the focused virtual library of **86** (Supporting information Table S2, page S9) compounds (**115–134**). These **20** compounds were then subjected to docking studies from where top **10** compounds (**115–119**, **120–121**, **127**, **130–131**, Table 5) based on their mean docking scores were selected for synthesis, the detailed docking studies are described in the next section. These NCEs were synthesized and evaluated for their PTP1B inhibitory potential as new leads as well

as for further validation of the Hypo-1. These molecules along with their predicted K_i and fit values on Hypo-1 are described in Table 5. Among these compounds top five compounds (**115–119**) were in the higher range (7.04–6.40) of fit value while the rest five compounds (**120–121**, **127**, **130–131**) showed lower fit values (5.68–5.22) as compared to the fit value (6.95) of the clinical compound **113** used as a reference compound [61]. The top two compounds **115** and **116** mapped very well with all features of Hypo-1 except one negatively ionizable function. The 4-methyl substitution of 2,4,6-trimethyl benzene sulphonamide group and N-benzyl substitution of compound **115** mapped on two

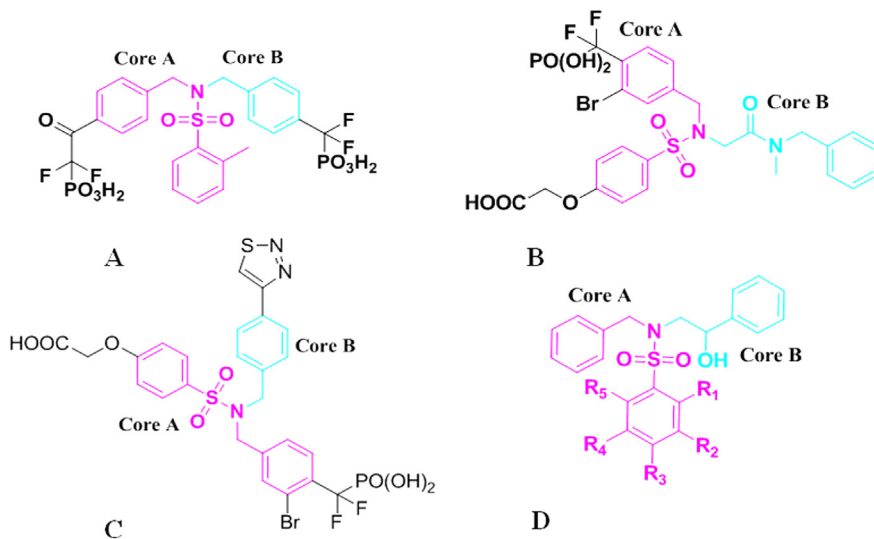


Fig. 4. Scaffolds from literature and designed core compounds. (A) The structures of the template scaffolds DFMP containing inhibitors of PTP1B (**113**, Affimax, IC_{50} 0.6 μ M) and (B) and (C) the compounds selected from literature (**114**, **114a**) [61,62]. (D) The core selected for further development as PTP1B inhibitor.

Table 5

The structures of ten designed ligands based on scaffold hopping protocol and pharmacophore mapping.

Comp. No	R ₁	Fit value	Act pred.	Comp. No	R ₁	Fit value	Act Pred.
115		6.91	0.130	120		5.8	1.76
116		6.91	0.129	121		5.95	1.17
117		6.6	0.268	127		5.75	1.88
118		7.04	0.096	130		5.66	2.29
119		6.85	0.148	131		5.6	2.29

HYDROPHOBIC features, while its $-\text{SO}_2$ group and the N-(2-hydroxy-2-phenylethyl) substitution mapped to one hydrogen bond acceptor and one ring aromatic features respectively. Similarly the compound **116** also mapped well with all features of this pharmacophore except one negatively ionizable function where two HYDROPHIC features mapped by N-benzyl and N-(2-hydroxy-2-phenylethyl) substitution with slightly higher displacement from their centroids, while the $-\text{OH}$ group of the N-(2-hydroxy-2-phenylethyl) and 2-Nitro benzenesulphonamide mapped to the one hydrogen bond acceptor and ring aromatic features respectively (Fig. 5).

2.6. Docking studies

In order to further validate the prioritized virtual molecules the docking studies were performed using Gold 3.0.1 and Molegro Virtual docker 4.0 (MVD 4.0) with almost similar scoring functions. The PDB ID-1AAK [60] was used in docking experiments for both the MVD 4.0 and Gold docking protocols and the mean values of these docking scores were considered to prioritize the top ten molecules for synthesis (Table 6) considering **113** and **114** as reference compounds [61,62]. The two ligands viz. **115** and **116** were explained in detail as a representative of this series. The ligands had good binding scores at the receptor level in both scoring functions Table 6.

2.7. Synthesis

In continuation of the above computational approaches and virtual screening of the focused library the top ten prioritized molecules were synthesized. The key intermediate of **3** was synthesized by the reaction of silica catalyzed regioselective epoxide opening of (\pm)-styrene oxide (**2**) by nucleophilic attack of

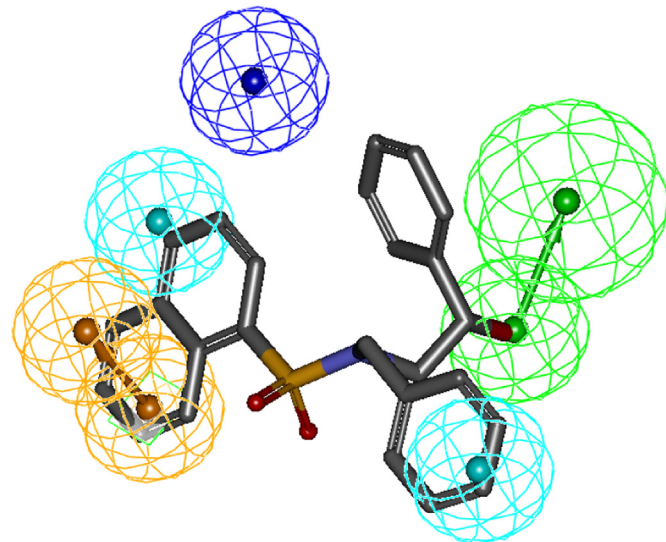


Fig. 5. Ligand pharmacophore mapping of designed compounds on Hypo-1. Pharmacophore alignment of predicted compound **115**.

benzylamine (**1**) to give intermediate (**3**) in 90% along with its corresponding regioisomer (**3a**) [66]. The desired β -aminol (**3**) was also reported by earlier [67] and used for the synthesis of the prioritized molecule **115–124** through substituted arylsulphonic acid, triethylamine and dry dichloromethane was used as a solvent (Scheme 1).

2.8. SAR studies and biological screening

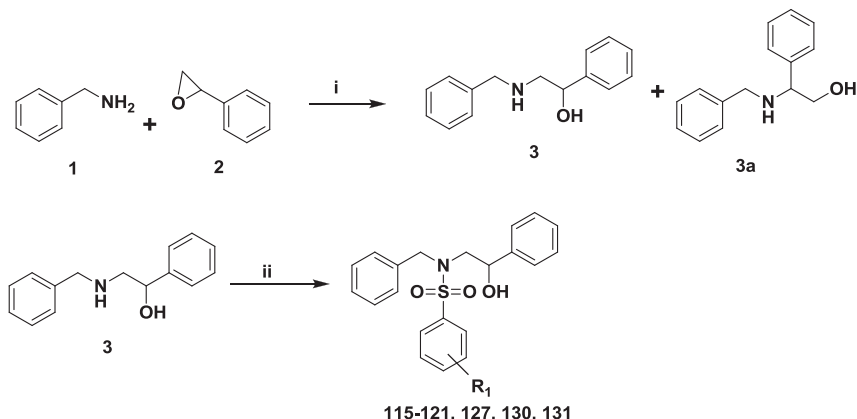
The PTP1B inhibitory activity for all the active and moderately active compounds was assessed for confirming the results predicted by preliminary in-silico studies. In order to determine the IC₅₀ of these compounds the % inhibition was measured at different concentrations. The IC₅₀ values were obtained from these results are presented in Table S4 and S5 in supporting information page S14. The IC₅₀ values of five top most active compounds were confirmed by reanalyzing the % inhibition of these compounds at the determined IC₅₀ values (Supporting information, Table S6, page S15) where approximately 50% inhibition was observed at the calculated IC₅₀ values from the dose response behavior. The top five compounds (**115–119**) exhibited good *in-vitro* inhibitory activity, with IC₅₀ values between 7.54 and 16.4 μM (Table 7).

Among the compounds where R₁ position is substituted by aryl sulphonyl group the most active was the one where aryl was 1-

Table 6

The binding scores of the top 10 compounds along with reference standard compounds used in analysis.

Ligand	Moldock score	Rerank score	Gold score	Mean docking scores
113	-146.652	-79.7862	68.36	-54.3337
114	-137.336	-89.8425	64.39	-54.2628
116	-131.69	-90.9309	63.77	-53.5963
119	-120.49	-97.9314	61.28	-52.9503
117	-129.725	-88.774	57.71	-52.6927
118	-127.832	-88.4691	53.3	-52.5448
120	-126.389	-83.5051	55.27	-52.3805
121	-123.976	-87.3485	53.69	-51.7054
131	-123.636	-84.7101	53.23	-51.5414
115	-121.533	-85.4492	54.01	-51.0964
130	-128.25	-76.6329	53.98	-50.9907
127	-117.125	-88.3041	52.14	-50.3031



Scheme 1. Reagents and conditions: (i) SiO₂, N₂ atm. for 24 h; (ii) ArSO₂Cl, TEA (1.2 eq.)/dry DCM.

naphthyl (**119**), this was followed in the order 2-nitro phenyl > 2,4,6-trimethyl phenyl > 3-carboxy phenyl > 3-trifluoromethyl phenyl > 8-quinoline > 4-trifluoromethyl phenyl > 2, 6-dimethyl phenyl > 3-thiophene > 2,5-dichloro phenyl. This variation in activity is possibly due to the variation in hydrophobicity and electronic factors which have already been analyzed through pharmacophore development. Moreover five of these compounds (**115–119**) showed promising activity not only *in-vitro* but also in STZ-s model *in-vivo*.

2.9. Binding modes of ligands

The binding modes of the two top most compounds (**115, 116**) with the target proteins PTP1B were analyzed by using the Molegro virtual docker 4.0 and the visualizer 3.0 in Discovery studio for Gold software. In order to validate the docking protocol the reference compound **113** and the co-crystallized ligand (BPPM) were docked in the binding site of PTP1B. The docking interactions of **113** at the binding site showed a similar binding pattern with the important binding site residues reported for the co-crystallized ligand (PDB ID 1AAC) as evident by the scoring functions (Table 6). The proximal part of the standard ligand (**113**) showed the interactions with Lys-120, Ser-216, Ala-217, Arg-221, Arg-218, Ile-221, Ser-215 similar to BPPM. In order to get more insight, the pharmacophoric mapping of the standard ligand was also considered for the identification of the interactions at the binding site and the results were integrated with the docking protocols (Fig. 6 A, B and C).

The top five designed scaffolds showed the GOLD fitness scores in the range of 53–63. The reference ligand (**114, 113**) from the scaffold hopping showed the hydrogen bond interactions with the Arg-24, Tyr-20, Gly-259, Ser-216 and Phe-182. The binding modes of the two top scoring ligands **115** and **116** are discussed in the sections below.

2.10. Ligand 115

The compound **115** showed interactions at the hydrophobic side of the template molecule, where 1-phenylpropan-1-ol showed the hydrophobic interactions with the half hydrophobic binding site with amino acid residues viz. Asp-181, Phe-182, Gln-262, Gln-220 and the Gln-266 (Fig. 7 A and B). The latter part of the template molecule showed strong van der Waals interactions along with the extensive network of hydrogen bonds may be the key reasons for the higher scores and probably the activity of the designed molecules. Its other important binding interactions included electrostatic interactions with the Arg-221, hydrogen bonds with the main chain nitrogen's of Ser-216, Arg-221, Ala-217,

Lys-220. The “pi–pi” stacking interactions with Tyr-46 along with the strong hydrogen bond interactions between i) the –OH functionality of 1-phenylpropan-1-ol fragment and the residues like Ser-215 Ala-217, Arg-221 and ii) the hydrophobic or pi–pi stacking interactions between 1-phenylpropan-1-ol fragment showed the strong interactions with Lys-116, Phe-182, and Tyr-46 along with the N-benzyl substitution also have added effect on these interactions.

Similarly the other molecule **116** also showed the hydrogen bond interactions between i) Arg-221, Gln-220, Ala-217, Ser-216 with sulphonamide fragment ii) the –OH function in 1-phenylpropan-1-ol showed the hydrogen bond interactions with Lys-120 and iii) the 2-Nitro benzene sulphonyl chloride fragment of the molecule showed strong hydrogen bonds with Arg-221, Gln-266 and the Phe-182. These strong hydrogen bonding and the van der Wall's interactions resulted in the higher binding scores of the designed scaffold than the reference ligand and as compared to the standard ligands in the literature (Fig. 8A and B).

3. In-vitro screening

The PTP-1B inhibitory activities of the synthesized compounds were determined, and the results were summarized in Table 7. Five (compound no. **115–119**) of these compounds exhibited effective *in-vitro* inhibitory activity, with IC₅₀ values around 7.54–16.4 μM. The PTP-1B activity was assessed for all the active and inactive compounds so as to confirm the results predicted by preliminary *in-silico* studies for the design of these compounds. The results shown in the table reveal the effects of the different substitutions at R₁ position the 2,4,6-trimethyl benzenesulfonamide, 2-nitrobenzenesulfonamide, 3-sulfamoyl benzoic acid, 3-trifluoromethyl, 1 –naphthalene were found active in the *in-vitro* PTP-1B inhibitory activity. The pharmacophore mapping also reveals the same while in the case of heterocyclic substitution of the benzene ring of the sulphonyl chloride with thiophene, quinoline substitutions reduces the activity. The different substituted benzene along with the chlorine, 4-trifluoromethyl and 2, 6-dimethyl also lack the mapping fit values and found inactive at PTP-1B *in-vitro* assay. The conclusion can be drawn from this study that different benzene substitutions gave the best result (Table 7). The blood glucose level in mg/dl for all the synthesized compounds at different time interval were represented in details in Supporting information Table S7 page S16.

In order to confirm the IC₅₀ of these compounds we had determined the % inhibition for different inhibitor concentration the IC₅₀ values obtained from these results were represented in Table 8.

Table 7

The representation of fit values and observed IC₅₀ values along with the STZ-s model results in terms of improvement in glucose tolerance on fasting blood glucose.

Comp. No	R ₁	IC ₅₀ μM ^a	STZ-S ^b		2-Deoxy-D-[3H]-glucose uptake (10 μg)
			5 h	24 h	
115		7.54 ± 0.40	-25.9	-28.4	62.50%**
116		8.32 ± 0.20	-22.5**	-28.4**	69.2%**
117		14.3 ± 0.45	-16.2*	-19.1*	31.14%
118		16.4 ± 0.28	-23.6***	-28.4***	44.30%
119		12.2 ± 0.36	-25.9***	-31.4***	32.1%**
120		45.9 ± 0.64	-4.07	-3.65	26.90%
121		58.1 ± 0.60	13.9	11.2	10.21%
127		46.6 ± 0.55	5.77	9	8.10%
130		74.2 ± 0.11	-12.3	-11	16.90%
131		57.5 ± 0.52	-14	-9	3.43%
Glibenclamide	—	—	-25.1***	-28.2***	—

^a IC₅₀ values are means ± SEM of series separate assays, each performed in triplicate.

^b Effect of synthetic compounds (100 mg/kg) and standard drug Glibenclamide (50 mg/kg) on the blood glucose levels at various time intervals. *p < 0.05; **p < 0.01; ***p < 0.001 vs. vehicle treated control.

3.1. Effect on glucose uptake

Effect of compounds (**115–124**) on glucose uptake was investigated in differentiated L6 myotubes and was found that compound **115** and **116** effectively enhance the glucose uptake at 10 μg/ml concentration (**Table 7**). Compound **115** and **116** showed an effect of 62.50 and 69.2% (p < 0.01) on glucose uptake in differentiated L6 myotubes.

3.2. In-vivo screening

3.2.1. Compound 115 improved the glucose tolerance on streptozotocin-induced diabetic rats

The results obtained from in vitro screening encouraged us to screen them on sucrose challenged streptozotocin-induced diabetic rats. It is illustrated in **Table 8** that compound **115–119** significantly improved the rise in postprandial hyperglycemia post sucrose challenged on streptozotocin-induced diabetic rat during 0–5 and 0–24 h respectively [68], whereas standard drug Glybenclamide showed an improvement of 25.1, 28.2% (p < 0.001), at 5 h and 24 h respectively.

3.2.2. Compound 115 improved the random blood glucose, fasting blood glucose, serum insulin, HOMA-index and OGTT of db/db mice

The results obtained from sucrose challenged streptozotocin-induced diabetic rats, encouraged us to further screen them in db/db mice. To elucidate the effect of compound **115**, db/db mice were orally gavaged for 15 consecutive days at 30 mg/kg dose level. It was observed that compound **115** significantly improves the random blood glucose level from day 7th which persisted till last day of experiment, whereas the reference drug rosiglitazone showed its effect from day 3rd till the end of the experiment (**Fig. 9a**).

The improvement on fasting blood glucose (**Fig. 9b**) was calculated to be around 35.5 and 52.5% (p < 0.01) whereas a decline of 28.4 and 41.3% (p < 0.01) in serum insulin (**Fig. 9c**) was observed by repeated oral gavages of compound **115** and rosiglitazone respectively. The improvement in fasting blood glucose and serum insulin leads to improvement in insulin resistance which was evident by decline in HOMA-index as showed in **Fig. 9d** which was calculated to be around 47.8 and 67.1% (p < 0.01). It was also found that compound **115** improved the oral glucose tolerance by 14.7% (p < 0.05) and 41.2% (p < 0.01), whereas rosiglitazone showed an improvement of 28.4 and 49.9% (p < 0.01) on day 10 and 15 respectively.

3.2.3. Compound 115 improved the serum lipid profile of db/db mice

The effect of compound **115** on serum lipid profile in db/db mice was also studied to investigate the additional beneficial effects of the compound. Repeated oral administration of compound **115** at 30 mg/kg dose significantly declined serum TG by 15.2% (p < 0.05), serum total cholesterol by 14.1% and enhances the level of serum HDL-c by 7.41%. Whereas the rosiglitazone, decline the serum TG and total cholesterol by 13.5 and 9.7% respectively whereas enhances the serum HDL-c by 10.3% (**Fig. 9g**). It was also observed that compound **115** showed a marked decline in body weight by 13.3% (p < 0.01), whereas the rosiglitazone showed an increase of 0.936% in body weight as compared to vehicle treated control group (**Fig. 9h**).

3.3. Compound 115 inhibits the preadipocyte differentiation significantly and showed promising anti-adipogenic activity

Considering the antidiabetic activity of the compound **115** in genetically diabetic and obese C57BL/KsJ-db/db mice, the compound **115** was further analyzed for its effect on adipocyte differentiation. MDI stimulates adipocyte differentiation as showed by Oil red O (ORO) staining in the 3T3-L1 cells. Whereas compound **115** reduced the MDI-stimulated lipid accumulation in a dose-dependent manner (**Fig. 10a**). Quantitative analysis of ORO staining indicated that MDI increases relative lipid contents more than 3-fold in 3T3-L1 preadipocytes compared with undifferentiated controls. MDI-induced lipid accumulation was reduced approximately 1.9 fold and 4 fold in the cells treated with 10 μM and 20 μM

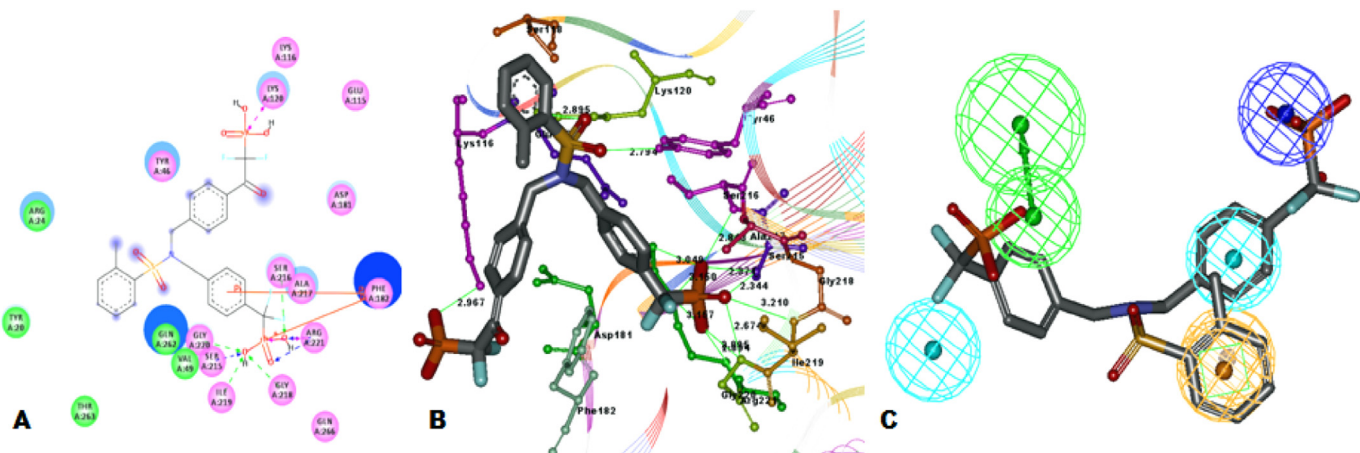


Fig. 6. Docking pose of **113** in PTP1B along with pharmacophore alignment. (A) The 2D representation of the hydrogen bonding and pi–pi stacking interactions of compound **113** at the binding site. (B) The molecular interactions of the standard compound **113** at the binding site (C) Pharmacophore alignment of the standard ligand compound **113** on Hypo-1 with the fit value of 6.95.

of compound **115**, respectively (Fig. 10b). While rosiglitazone increased 1.2 fold adipogenesis at 10 μ M concentration as compared with MDI induced control cells. As revealed in the Oil-red O staining, compound **115** inhibits the preadipocyte differentiation significantly and showed promising anti-adipogenic activity. Further to assess effect of compound **115** on cell viability, 3T3-L1 cells were treated with 5–20 μ M of compound **115** and MTT assay was carried out. The compound was nontoxic to cells at all the concentrations from 5 μ M to 20 μ M. The representative figure for the same and the protocol was included in the supplementary information figure S3 page S19.

\sim 3.61, \sim 2.91, \sim 2.69 and \sim 3.59 ($p < 0.05$) in compound **115** treated mice where as \sim 4.85, \sim 4.46, \sim 4.24 and \sim 4.55 ($p < 0.001$) fold increase in rosiglitazone treated mice group respectively (Fig. 11a). Likely in liver of db/db mice treated with compound **115** and rosiglitazone mRNA expressions of IRS2, PI3K, AKT2 and GLUT2 was increased to the fold of \sim 3.83, \sim 2.53, \sim 2.05, \sim 1.83 ($p < 0.05$) and \sim 4.66, \sim 3.86, \sim 3.22, \sim 2.90 ($p < 0.001$) respectively (Fig. 11d). Further it was also observed that compound **115** and rosiglitazone effectively decreased the mRNA expression level of PTPN1 along with an increase of AMPK and PPAR- α expression in the skeletal muscle and liver of db/db mice as compared to the vehicle treated control group (Supplementary information Fig. S4 (A and B respectively) on page S19).

3.4. Inhibition of PTP1B with compound 115 improved the insulin signaling related gene expression in skeletal muscle and liver of db/db mice

Inhibition of PTP1B with compound **115** significantly enhanced the insulin signaling in skeletal muscle and liver of db/db mice as compared to vehicle treated control group. In skeletal muscle the expression of IRS1, PI3K, AKT2 and GLUT4 was increased to the fold of

3.5. Inhibition of PTP1B with compound 115 increased IRS phosphorylation and increased IRS associated PI3K activity in skeletal muscle and liver of db/db mice

It was found that protein levels of p-IRS1, p-akt and Glut4 was increased to the fold of ~2.54, ~1.66, ~1.49 and ~3.24, ~2.86, ~2.55 in skeletal muscle of db/db mice treated with compound 115 and

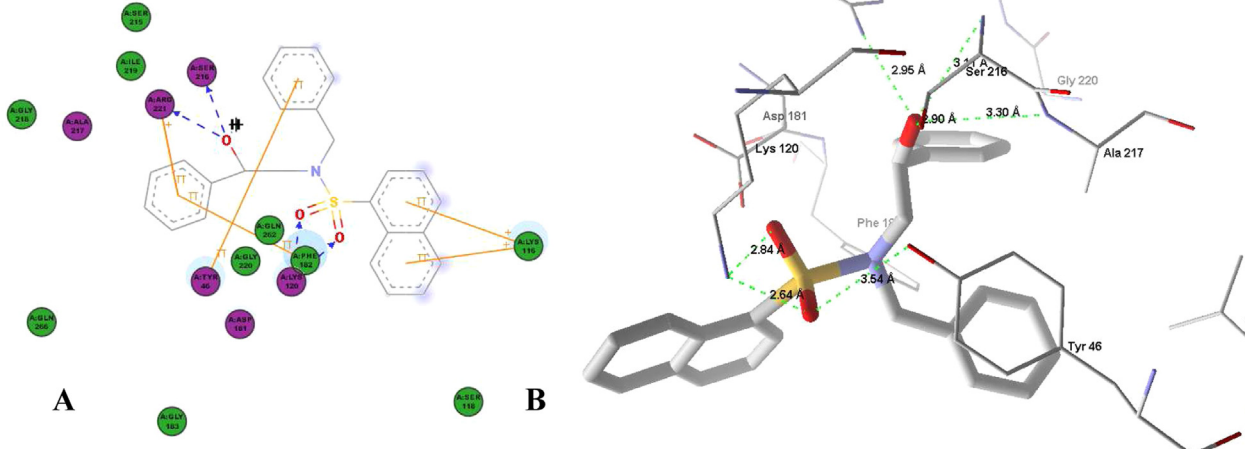


Fig. 7. Docking pose of compound **115** in PTP1B. (A) The 2D interactions of the top ranked compound **115** showing all required hydrogen bond interactions. (B) The molecular interactions of the compound **115** at the PTP1B binding site.

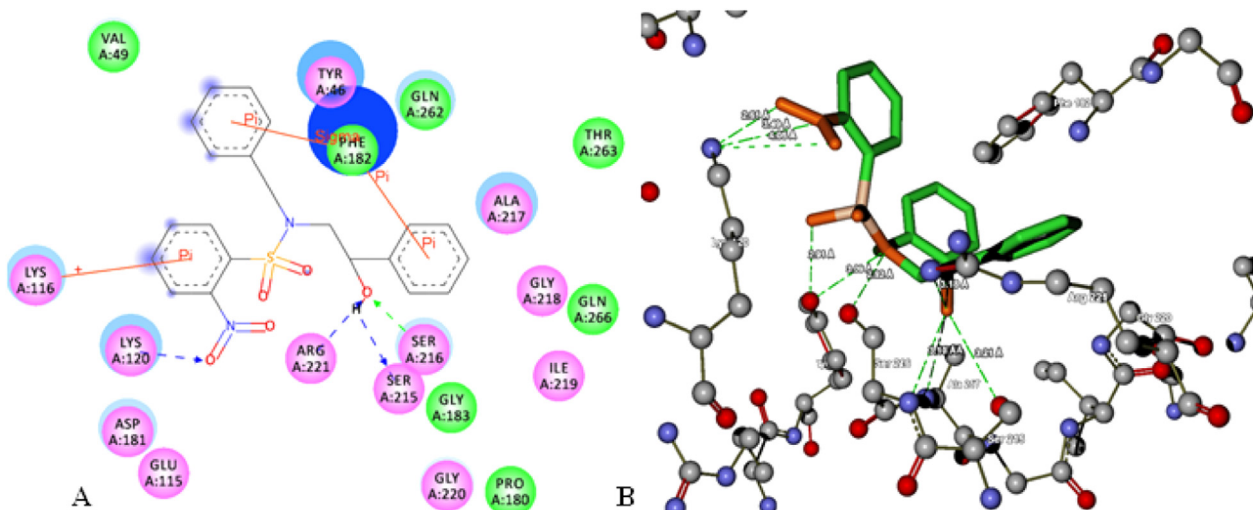


Fig. 8. The molecular interactions of **116** at the binding site. (A) 2D interactions of the best conformation selected from best docked pose using Gold software (B) 3D interactions represented in Molegro virtual docker pose organizer.

rosiglitazone respectively. Whereas the protein level of p-IRS2, p-akt, Glut2 was increased to the extent of ~2.42, ~1.46, ~1.20 and ~3.04, ~2.05, ~1.32 folds in liver of db/db mice treated with compound **115** and rosiglitazone respectively.

4. Discussion

Type 2 diabetes is associated with insulin resistance, possibly because of attenuated insulin from its receptor molecules. Balance between tyrosine phosphorylation and dephosphorylation of insulin receptor (IR) and its primary substrate, namely the insulin receptor substrate (IRS-1/2) proteins regulates the insulin mediated signal transduction. PTP1B is a key element in the negative regulation of the insulin signaling pathway and inhibition of this enzyme is predicted to be an excellent, novel therapeutic target for type 2 diabetes and obesity [69]. In this study we demonstrated that compound **115** effectively inhibit the PTP1B and stimulate the glucose utilization by L6 myotubes. The compound **115** also showed significant antidiabetic, antidiabetic and antiadipogenic properties. The PTP1B inhibition by compound **115** results in enhanced insulin sensitivity and increased insulin stimulated phosphorylation of downstream signaling proteins and thereby facilitates glucose uptake in skeletal muscle and liver which presumably resulted in the lowering of blood glucose level. In order to address the possible mechanism of action underlying the effect of compound **115**, mRNA levels of certain genes involved in insulin signaling were determined. The analysis demonstrated that the treatment of compound **115** caused a significant increase in mRNA levels of IRS-1, PI3K, AKT2, Glut4, in skeletal muscle (Fig. 11a) along with IRS2, PI3K, AKT2, Glut2 in liver (Fig. 11d) as compared to

vehicle treated control group. Western blot analysis of skeletal muscle and liver demonstrated that the expression of intermediate proteins of insulin signaling were also increased as compared to control group. Inhibition of PTP1B by compound **115** prolonged the insulin signaling which was observed with the significant increase in protein expression of phosphorylated IRS1 and IRS2 in skeletal muscle and liver respectively as showed in Fig. 11b and e. The stimulation of IR kinase activity [70] induced the phosphorylation of endogenous IRS-1 and IRS-2 which triggers the signal transduction by activating downstream targets such as phosphatidylinositol-3 kinase (PI3K) and Akt. The Akt is also an important mediator of biological functions of insulin. Activated Akt induces the translocation of glucose transporter (GLUT4/2) from the intracellular compartment vesicle to the plasma membrane, leading to increased cellular glucose uptake [71–73]. In the same context western blot analysis also revealed that consecutive oral gavages of compound **115** increased expression of the phosphorylated Akt in both tissues along with glucose transporter protein i.e. GLUT4 in skeletal muscle and GLUT2 in liver as showed in Fig. 11d and e. Therefore, it may be concluded that increased expression of phosphorylated IRS1 and IRS2, phosphorylated akt and Glut4 and Glut2 is a consequence of inhibition of PTP1B by the compound **115** which further increased the insulin signaling and sensitivity in the skeletal muscle and liver respectively.

Many reports indicate that activation of AMPK and PPAR pathway results in the improvement on insulin sensitivity, glucose uptake, hepatic glucose output, fatty acid oxidation and lipogenesis [74–77]. It was observed that compound **115** significantly declined the serum triglyceride level and body weight of db/db mice as compared to the standard drug rosiglitazone. Compound **115** also effectively upregulated the mRNA expression of AMPK and PPAR α in the skeletal muscle and liver of the db/db mice (Fig S4) which may also be correlated with the antidiabetic and antidiabetic effect of the compound **115**. We then studied the antiadipogenic effect of compound **115** in terms of lipid accumulation and we observed that compound **115** effectively decreased the accumulation of lipid droplets in 3T3-L1 preadipocytes. These results suggest that the compound **115** in addition to the inhibition of PTP1B may also activate AMPK and PPAR pathway which may lead to the observed with the improved insulin signaling, fasting blood glucose, random blood glucose, glucose tolerance, lipid profile and body weight.

Table 8

The percentage inhibition of the PTP1B by test compounds from triplicate experiments.

Sr. no.	Compound code	% Inhibition at different inhibitor concentration					IC_{50} μM
		1 μM	3 μM	5 μM	10 μM	15 μM	
1	115	4.6	18.9	30.0	81.5	89.4	7.54
2	116	4.1	10.2	29.1	76.3	79.9	8.32
3	117	2.1	11.2	19.1	32.5	53.3	14.3
4	118	1.1	8.2	19.1	25.1	46.4	16.4
5	119	0.6	5.9	15.1	37.5	64.4	12.2

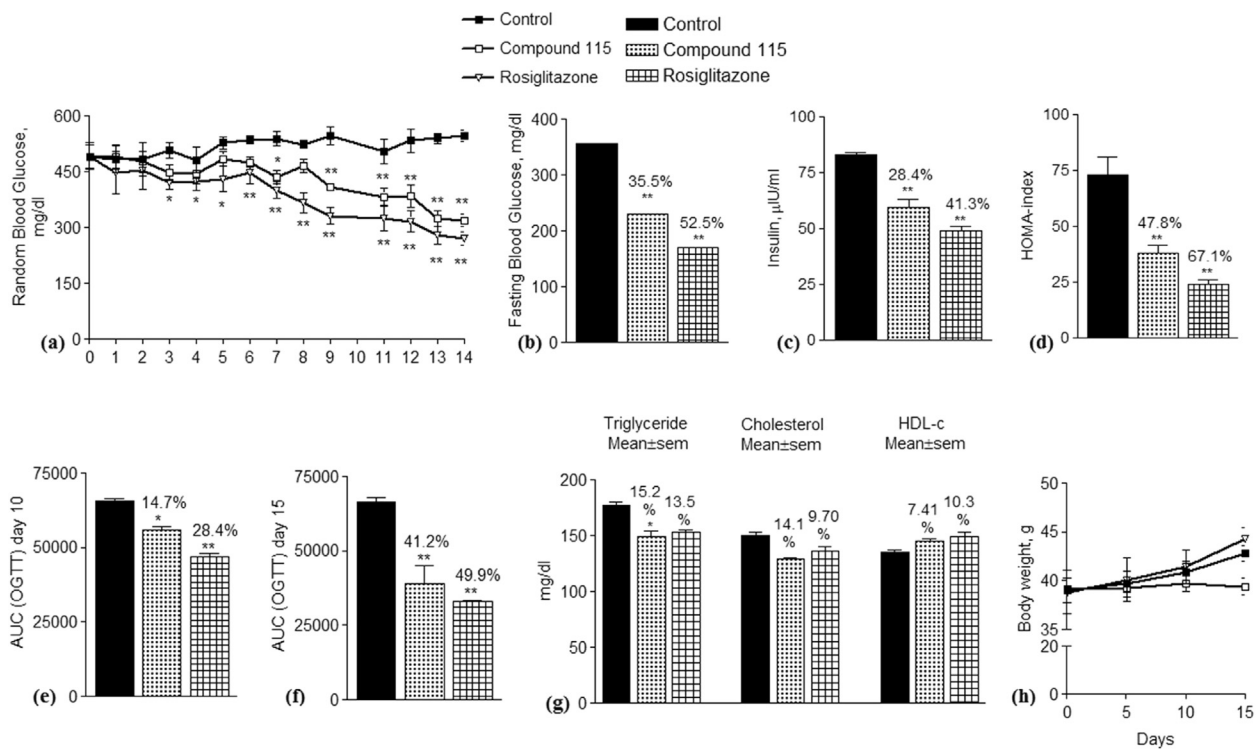


Fig. 9. Treatment of compound 115 leads to increased insulin sensitivity. Random blood glucose (a), fasting blood glucose (b), insulin (c), HOMA-index (d), OGTT 10 day (e), OGTT 15 day (f), lipid profile (g), body weight (h) in db/db mice. The values are mean \pm S.E. Significance * $p < 0.05$, ** $p < 0.01$, *** $p < 0.001$.

5. Oral bioavailability studies of compound 115 in rat

The data obtained for albumin interaction also supports the mode of transport in blood, absorption, distribution and possible bioavailability of these compounds ([Supporting information Section](#)

9.1–9.3). Therefore oral bioavailability of the compound 115 was assessed in rat at 30 mg/kg dose. [Fig. 12](#) showed the compound 115 mean plasma concentration vs. time plots of the IV and Oral pharmacokinetic studies. Oral bioavailability was found ~10.29% after 30 mg/kg oral dosing and 3 mg/kg IV dosing ([Table 9](#)). The compound

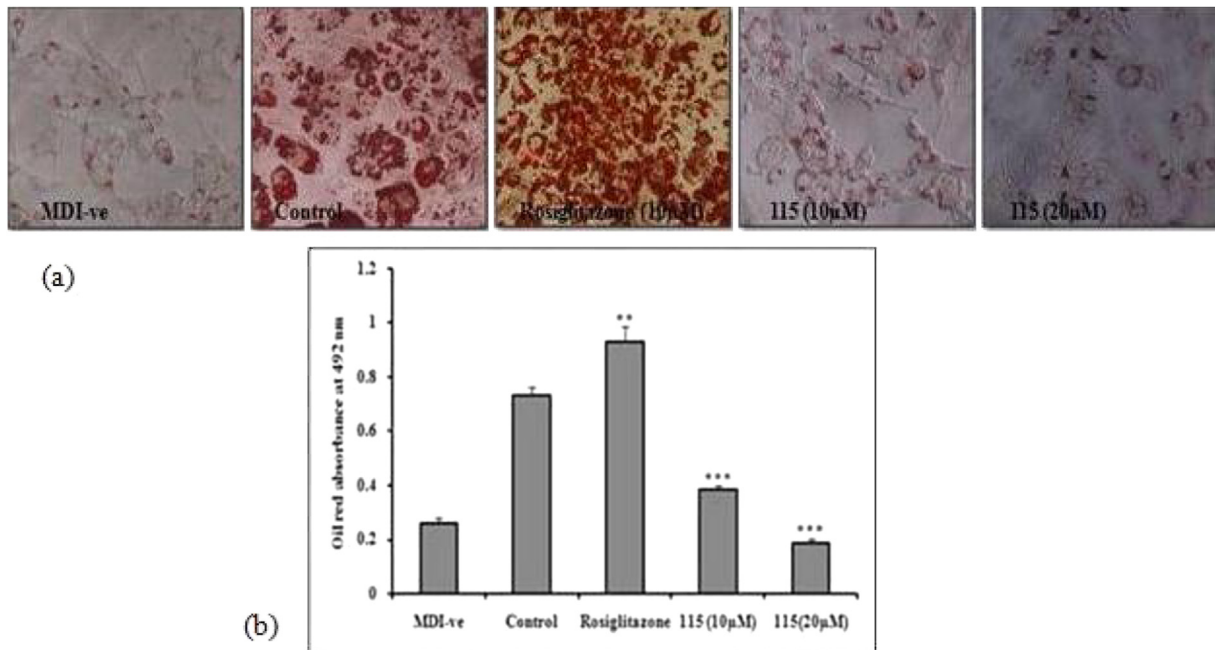


Fig. 10. Effect of compound 115 on MDI-induced adipogenesis. (a) and (b) Effects of compound 115 on MDI-induced adipogenesis in 3T3-L1 preadipocytes, compound 115 inhibited differentiation of 3T3-L1 preadipocytes as indicated by staining with Oil Red O solution. Data are the mean \pm S.D., $n = 3$ and $p < 0.001$ when compared with MDI induced control group. (For interpretation of the references to colour in this figure legend, the reader is referred to the web version of this article.)

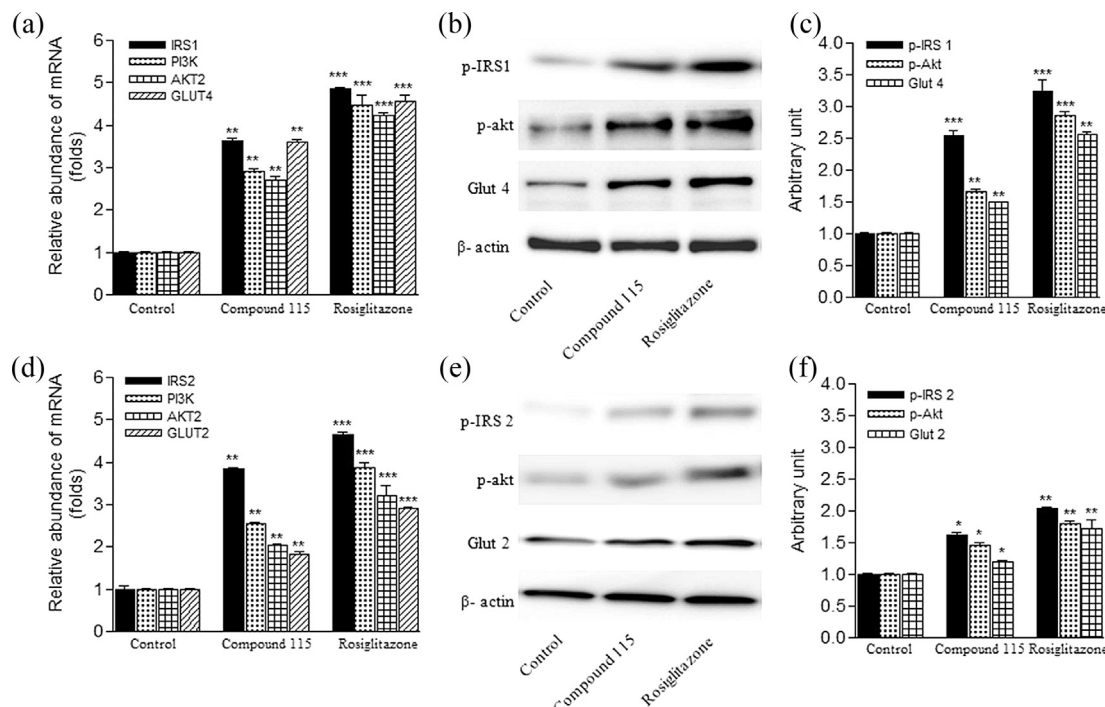


Fig. 11. Inhibition of PTP1B by compound 115 results in significant increase in mRNA expression of certain genes and protein levels involved in insulin signaling. The mRNA expression of IRS 1, PI3K, AKT2 and GLUT4 (a), protein levels of p-IRS1, p-akt, Glut4 (b) and their densiometric analysis (c) in skeletal muscle of db/db mice. The mRNA expression of IRS 2, PI3K, AKT2 and GLUT2 (d), protein levels of p-IRS2, p-akt, Glut2 (e) and their densiometric analysis (f) in liver of db/db mice. The mRNA level of IRS-1, PI3K, AKT2, Glut4 in skeletal muscle and IRS-2, PI3K, AKT2, Glut2 in liver were quantified by quantitative Real-Time PCR using specific primers. Level of proteins was assessed by western blot analysis, 40 µg of protein was resolved on SDS-PAGE and immunoblotted with antibodies against p-IRS1, p-IRS2, p-akt, Glut4, Glut2 and β-actin. All the experiments were repeated three times and values are means ± SEM of three independent experiments. All blots shown were representatives of the indicated groups and the densitometric analyses of the same are provided. **p* < 0.05, ***p* < 0.01, ****p* < 0.001.

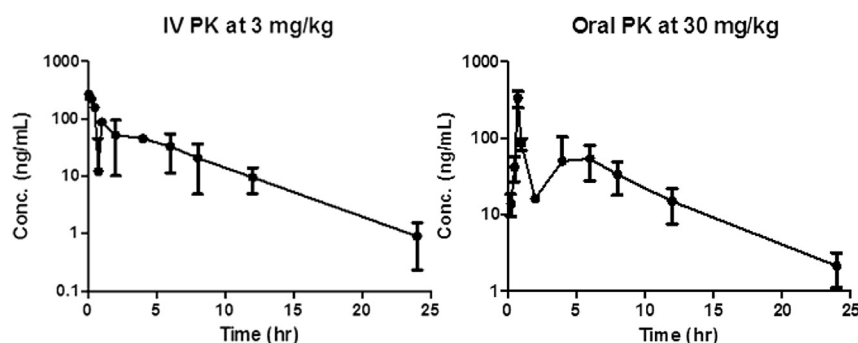


Fig. 12. Plasma concentration–time curves of compound 115 in rat after oral administration of 30.0 mg/kg; and i.v. administration of 3.0 mg/kg.

was detected in the plasma up to 24 h after oral and IV dosing. In oral compound showed rapid absorption within 45 min immediately after dosing. Half life of the compound was found 4.2 h after oral dosing suggested extended pharmacodynamic action (Fig. 12).

Table 9
Pharmacokinetic parameters of compound 115 in rats.

Parameters	IV (3 mg/kg)	Oral (30 mg/kg)
C _{max} (ng/mL)	266.40 ± 56.50	330.23 ± 81.08
T _{max} (h)	0.083	0.75
AUC _{0-∞} (h*ng/mL)	595.25 ± 134.32	612.88 ± 156.27
V _d (L/kg)	23.21 ± 0.89	29.40 ± 0.47
Cl (L/h/kg)	5.01 ± 0.33	5.06 ± 0.15
t _{1/2} (h)	3.22 ± 0.67	4.18 ± 0.97
MRT (h)	4.27 ± 0.22	6.62 ± 0.72
F (%)	—	10.29

6. Conclusion

In the present study, an efficient virtual screening has been performed using a HypoGen-based pharmacophore, scaffold hopping and docking technique for discovering novel PTP1B inhibitors. The best pharmacophore model provided a statistically significant correlation of 0.94 (rms = 0.8) and explained about 90% PTP1B inhibitory activity variation in the training set compounds. The best pharmacophore model has also well estimated PTP1B inhibitory activities of the test set compounds with overall predictive correlation (*r*) of 0.811 and explained about 70% PTP1B inhibitory activity variation. In addition, this model predicted very well diverse PTP1B inhibitors under clinical trials. This pharmacophore based modeling along with the scaffold hopping techniques provided novel potent PTP1B inhibitors. The twenty prioritized NCEs were analyzed for their molecular interactions at

the receptor site and then the top ten NCEs were synthesized and subsequently tested for in-vitro PTP1B assay and in-vivo STZ assay. Among these five compounds (**115–119**) were found highly active as compared to remaining compounds and the most active compound **115** was tested in C57BL/KsJ-db/db mice in-vivo model. This compound **115** significantly improved OGTT along with the fasting and random blood glucose level. The treatment by the compound **115** significantly improved the insulin resistance and insulin signaling by restoring the insulin level and normalizing the serum lipid profile. It also augmented the insulin action by modulating the expression of genes involved in insulin signaling like IRS 1–2, PI3K, PTPN1, Akt2, AMPK and PPAR- α . Western blot analysis of both skeletal muscle and liver demonstrated that proteins and intermediate enzymes of insulin signaling were also increased as compared to the control group. The effect of the compound **115** was also investigated for anti-adipogenic effect on 3T3L-1 cells. The compound **115** inhibited MDI induced lipid accumulation in a dose-dependent manner. The oral bioavailability of compound **115** was ~10.29% after 30 mg/kg oral dosing and 3 mg/kg IV dosing and compound was detected in the plasma up to 24 h after oral and IV dosing. The half life of the compound was found 4.2 h after oral dosing suggested extended pharmacodynamic action. On the basis of the data derived from these diverse biological experiments, one novel lead, namely compound **115**, with desirable physicochemical properties and bioavailability in recent future may provide the basis for the design of novel PTP1B inhibitors for the treatment of type-II diabetes mellitus.

7. Materials and methods

7.1. Pharmacophore modeling

The selection of the suitable molecules with the structural diversity is important for the generation of the pharmacophore model. In order to fulfill the requirement the four different series comprising of **112** molecules with diversity in structural features and wide range of activities were selected. The activity in terms of K_i of these compound's ranged from 0.00068 μm to 280 μm spanning 5 orders of difference reported by Zhan-Kui Wan et al. [78–81]. In this study, 30 compounds were selected in training set (Table 1) and the rest of the compounds (82) were retained in the test set (Table 1, Supporting information, Page S3–S7).

7.2. Pharmacophore generation

The 30 PTP1B inhibitors selected in the training set were used for the pharmacophore generation. All the compounds were drawn in the CATALYST 2D/3D sketcher and energy minimized using the Charm-m force field in the Discovery studio 2.0. The total no of 250 conformations was generated incorporating the best-quality conformations with the energy 20 kcal/mol of the above the estimated global minimum for each molecule. The most probable features for the dataset were chosen from the feature mapping protocol incorporated in the software and the four features were selected as the most found features for the generation of HypoGen model viz. Hydrogen Bond Acceptor (HBA), Hydrophobic Feature (HY), Negative Ionizable (NI) and Ring Aromatic (RA). The HypoGen algorithm implemented in the Discovery Studio (DS) 2.0 program package (Accelrys, San Diego, CA) was used for the pharmacophore modeling. In the HypoGen run, ten pharmacophore hypotheses were generated and the top-ranked hypothesis was used for subsequent virtual screening. The top-ranked hypothesis contains one Hydrogen bond acceptor, two Hydrophobe, one Negative ionizable and one Ring aromatic feature sufficient to explain the hypothesis based on the cost value

analysis. The cost of the HypoGen algorithm indicates the total number of binary bits required for the generation of the particular pharmacophore hypothesis. The recommended values of residual, weight, and configuration costs are ≥ 40 , ≤ 2 , and ≤ 17 , respectively. Further quality assessment and validation of the pharmacophore model was done using the test set compounds, which were kept apart during the model development process. The 82 compounds retained in the test set were taken to estimate the quality of the best pharmacophore model. The 82 compounds were classified on the basis of their activity as highly active 0.00068 μm –3 μm (+++), moderately active 3.8 μm –160 μm (++) and least active 230 μm –280 μm (+).

7.3. Target structure preparation

In this study, we used two crystal structure of PTP1B complexed with an inhibitor molecule. 1AAX co-complexed with sulfamic acid moiety. The 3D coordinates of the enzymes were obtained from the PDB and it was further processed by removing the water molecules and other heteroatoms than the ligand. The hydrogen was added to a protein molecule along with the minimization by using protein minimization module available in the Discovery studio 2.0. The output of the minimization process was used for the docking process.

7.4. Molecular docking for PTP1B inhibitors

The compounds with the pharmacophore query were docked in the binding site of the PTP1B by the two docking programs viz. Molegro virtual docker and GOLD. The PDB ID 1AAX [60] was used for the docking experiments considering the binding site region around Arg-221 using the default protocols by these two softwares [82,83]. High gold scores and the rerank scores in the docking experiments indicates the good binding affinities of the ligands in the binding site. In the case of GOLD the protocol was set to retrieve top 10 ligands with best scores for analyzing the ligands for further studies.

7.5. Biological methods, Pharmacokinetic evaluation and BSA analysis of compounds

These protocols were represented in the Supporting information from page S19–S27.

Notes

The authors declare no competing financial interest.

Acknowledgments

The authors acknowledge the technical assistance by Ms. Vipasha Shukla, Mr. A. S. Kushwaha, Z. Ali and are thankful to the Sophisticated Analytical Instrument Facility (SAIF) department of CSIR-Central Drug Research Institute, Lucknow for providing the spectroscopic data. Two of us V.M.B. Y.S.C. and S.G. are thankful to the Indian Council of Medical Research, New Delhi for the financial assistance in the form of a fellowship. ANG acknowledges financial support from CSIR NWP BSC0102 "Thunder Project". The CSIR-CDRI communication number to this manuscript is 8809.

Appendix A. Supplementary data

Supplementary data related to this article can be found at <http://dx.doi.org/10.1016/j.ejmech.2014.09.097>.

References

- [1] A. Alonso, J. Sasin, N. Bottini, I. Friedberg, A. Osterman, A. Godzik, T. Hunter, J. Dixon, T. Mustelin, Protein tyrosine phosphatases in the human genome, *Cell* 117 (2004) 699–711.
- [2] B.G. Neel, N.K. Tonks, Protein tyrosine phosphatases in signal transduction, *Curr. Opin. Cell Biol.* 9 (1997) 193–204.
- [3] T. Hunter, Signaling-2000 and beyond, *Cell* 100 (2000) 113–127.
- [4] N.K. Tonks, B.G. Neel, Combinatorial control of the specificity of protein tyrosine phosphatases, *Curr. Opin. Cell Biol.* 13 (2001) 182–195.
- [5] K.R. Schiller, L.J. Mauro, Tyrosine phosphatases as regulators of skeletal development and metabolism, *J. Cell Biochem.* 96 (2005) 262–277.
- [6] P. Blume-Jensen, T. Hunter, Oncogenic kinase signaling, *Nature* 411 (2001) 355–365.
- [7] J. Montalibet, B.P. Kennedy, Therapeutic strategies for targeting PTP1B in diabetes, *Drug Discov. Today Ther. Strateg.* 2 (2005) 129–135.
- [8] W.S. Cook, R.H. Unger, Protein tyrosine phosphatase 1B: a potential leptin resistance factor of obesity, *Dev. Cell* 2 (2002) 385–387.
- [9] K.A. Kenner, E. Anyanwu, J.M. Olefsky, J. Kusari, Protein-tyrosine phosphatase 1B is a negative regulator of insulin- and insulin-like growth factor-I-stimulated signaling, *J. Biol. Chem.* 271 (1996) 19810–19816.
- [10] B.J. Goldstein, F. Ahmad, W. Ding, P.M. Li, W.R. Zhang, Regulation of the insulin signaling pathway by cellular protein-tyrosine phosphatases, *Mol. Cell Biochem.* 182 (1998) 91–99.
- [11] B.P. Kennedy, C. Ramachandran, Protein tyrosine phosphatase-1B in diabetes, *Biochem. Pharmacol.* 60 (2000) 877–883.
- [12] M. Elchebly, P. Payette, E. Michaliszyn, W. Cromlish, S. Collins, A.L. Loy, D. Normandin, A. Cheng, J. Himms-Hagen, C.C. Chan, C. Ramachandran, M.J. Gresser, M.L. Tremblay, B.P. Kennedy, Increased insulin sensitivity and obesity resistance in mice lacking the protein tyrosine phosphatase-1B gene, *Science* 283 (1999) 1544–1548.
- [13] L.D. Klaman, O. Boss, O.D. Peroni, J.K. Kim, J.L. Martino, J.M. Zabolotny, N. Moghal, M. Lubkin, Y.B. Kim, A.H. Sharpe, A. Stricker-Krongrad, G.I. Shulman, B.G. Neel, B.B. Kahn, Increased energy expenditure, decreased adiposity, and tissue-specific insulin sensitivity in protein-tyrosine phosphatase-1B-deficient mice, *Mol. Cell Biol.* 20 (2000) 5479–5489.
- [14] C.M. Rondinone, J.M. Trevillyan, J. Clampit, R.J. Gum, C. Berg, P. Kroeger, L. Frost, B.A. Zinker, R. Reilly, R. Ulrich, M. Butler, B.P. Monia, M.R. Jirousek, J.F. Waring, Protein tyrosine phosphatase 1B reduction regulates adiposity and expression of genes involved in lipogenesis, *Diabetes* 51 (2002) 2405–2411.
- [15] M. Na, W.K. Oh, Y.H. Kim, X.F. Cai, S. Kim, B.Y. Kim, J.S. Ahn, Inhibition of protein tyrosine phosphatase 1B by diterpenoids isolated from Acanthopanax koreanum, *Bioorg. Med. Chem. Lett.* 16 (2006) 3061–3064.
- [16] J.N. Andersen, O.H. Mortensen, G.H. Peters, P.G. Drake, L.F. Iversen, O.H. Olsen, H.S. Jansen, P.G. Andersen, N.K. Tonks, N.P.H. Moller, Structural and evolutionary relationships among protein tyrosine phosphatase domains, *Mol. Cell Biol.* 21 (2001) 7117–7136.
- [17] A.P. Combs, E.W. Yue, M. Bower, P.J. Ala, B. Wayland, B. Douty, A. Takvorian, P. Polam, Z. Wasserman, W. Zhu, M.L. Crawley, J. Pruitt, R. Sparks, B. Glass, D. Modi, E. McLaughlin, L. Bostrom, M. Li, L. Galya, K. Blom, M.I. Hillman, L. Gonville, B.G. Reid, M. Wei, M. Becker-Pasha, R. Klabe, R. Huber, Y. Li, G. Hollis, T.C. Burn, R. Wynn, P. Liu, B. Metcalf, Structure-based design and discovery of protein tyrosine phosphatase inhibitors incorporating novel isothiazolidinone heterocyclic phosphotyrosine mimetics, *J. Med. Chem.* 48 (2005) 6544–6548.
- [18] T.O. Johnson, J. Ermolieff, M.R. Jirousek, Protein tyrosine phosphatase 1B inhibitors for diabetes, *Nat. Rev. Drug Discov.* 1 (2002) 696–709.
- [19] R. Hooft van Huijsduijnen, S. Walchli, M. Ibbersen, A. Harrenga, Protein tyrosine phosphatases as drug targets: PTP1B and beyond, *Expert Opin. Ther. Targets* 6 (2002) 637–647.
- [20] X. Espanol, S. Walchli, R. Pescini-Gobert, M. El Alama, M.L. Curchod, N. Gullu-Isler, R. Hooft van Huijsduijnen, Pulling strings below the surface. Hormone receptor signaling through inhibition of protein tyrosine phosphatases, *Endocrine* 15 (2001) 19–28.
- [21] D. Barford, A.J. Flint, N.K. Tonks, Crystal structure of human protein tyrosine phosphatase 1B, *Science* 263 (1994) 1397–1404.
- [22] M.R. Groves, Z.J. Yao, P.P. Roller, T.R. Burke Jr., D. Barford, Structural basis for inhibition of the protein tyrosine phosphatase 1B by phosphotyrosine peptide mimetics, *Biochemistry* 37 (1998) 17773–17783.
- [23] P. Huang, J. Ramphal, J. Wei, C. Liang, B. Jallal, G. McMahon, C. Tang, Structure-based design and discovery of novel inhibitors of protein tyrosine phosphatases, *Bioorg. Med. Chem.* 11 (2003) 1835–1849.
- [24] M.A. Blaskovich, H.O. Kim, Recent discovery and development of protein tyrosine phosphatase inhibitors, *Expert Opin. Ther. Pat.* 12 (2002) 871–905.
- [25] G. Scapin, S.B. Patel, J.W. Becker, Q. Wang, C. Desponts, D. Waddleton, K. Skorey, W. Cromlish, M. Bayly, C. Therien, J.Y. Gauthier, C.S. Li, C.K. Lau, C. Ramachandran, B.P. Kennedy, E. Asante-Appiah, The structural basis for the selectivity of benzotriazole inhibitors of PTP 1B, *Biochemistry* 42 (2003) 11451–11459.
- [26] E. Asante-Appiah, S. Patel, C. Dufresne, P. Roy, Q. Wang, V. Patel, R.W. Friesen, C. Ramachandran, J.W. Becker, Y. Leblanc, B.P. Kennedy, G. Scapin, The structure of PTP1B in complex with a peptide inhibitor reveals an alternative binding mode for bisphosphonates, *Biochemistry* 41 (2002) 9043–9051.
- [27] P.J. Ala, L. Gonville, M. Hillman, M. Becker-Pasha, E.W. Yue, B. Douty, B. Wayland, P. Polam, M.L. Crawley, E. McLaughlin, R.B. Sparks, B. Glass, A. Takvorian, A.P. Combs, T.C. Burn, G.F. Hollis, R. Wynn, Structural insights into the design of nonpeptidic isothiazolidinone-containing inhibitors of protein-tyrosine phosphatase 1B, *J. Biol. Chem.* 281 (2006) 38013–38021.
- [28] A.P. Combs, Recent advances in the discovery of competitive protein tyrosine phosphatase 1B inhibitors for the treatment of diabetes, obesity, and cancer, *J. Med. Chem.* 53 (2010) 2333–2344.
- [29] A.P. Combs, W. Zhu, M.L. Crawley, B. Glass, P. Polam, R.B. Sparks, D. Modi, A. Takvorian, E. McLaughlin, E.W. Yue, Z. Wasserman, M. Bower, M. Wei, M. Rupar, P.J. Ala, B.M. Reid, D. Ellis, L. Gonville, T. Emm, N. Taylor, S. Yeleswaram, Y. Li, R. Wynn, T.C. Burn, G. Hollis, P.C. Liu, B. Metcalf, Potent benzimidazole sulfonamide protein tyrosine phosphatase 1B inhibitors containing the hetero-cyclic (S)-isothiazolidinone phosphotyrosine mimetic, *J. Med. Chem.* 49 (2006) 3774–3789.
- [30] S. Zhang, Z.Y. Zhang, PTP1B as a drug target: recent developments in PTP1B inhibitor discovery, *Drug Discov. Today* 12 (2007) 373–381.
- [31] S. Lee, Q. Wang, Recent development of small molecular specific inhibitor of protein tyrosine phosphatase 1B, *Med. Res. Rev.* 27 (2007) 553–573.
- [32] R.S. Ahima, H.R. Patel, N. Takahashi, Y. Qi, S.M. Hileman, M.A. Zasloff, Appetite suppression and weight reduction by a centrally active aminosterol, *Diabetes* 51 (2002) 2099–2104.
- [33] M. Zasloff, J.I. Williams, Q. Chen, M. Anderson, T. Maeder, S. Jones, W. Kinney, K. Cheshire, M. McLane, A spermine-coupled cholesterol metabolite from the shark with potent appetite suppressant and antidiabetic properties, *Int. J. Obes. Relat. Metab. Disord.* 25 (2000) 689–697.
- [34] N. Takahashi, Y. Qi, H.R. Patel, R.S. Ahima, A novel aminosterol reverses diabetes and fatty liver disease in obese mice, *J. Hepatol.* 41 (2004) 391–398.
- [35] K.A. Lantz, S.G. Hart, S.L. Plane, M.F. Roitman, I.A. Ruiz-White, H.R. Wolfe, M.P. McLane, Inhibition of PTP1B by trodusquemine (MSI-1436) causes fat-specific weight loss in diet-induced obese mice, *Obesity* 8 (2010) 1516–1523.
- [36] A.K. Gupta, S.S. Bhunia, V.M. Balaramnavar, A.K. Saxena, Pharmacophore modelling, molecular docking and virtual screening for EGFR (HER 1) tyrosine kinase inhibitors, *SAR QSAR Environ. Res.* 3 (2011) 239–263.
- [37] S.S. Chaudhaery, K.K. Roy, N. Shakya, G. Saxena, S.R. Sammi, A. Nazir, C. Nath, A.K. Saxena, Novel carbamates as orally active acetylcholinesterase inhibitors found to improve scopolamine-induced cognition impairment: pharmacophore-based virtual screening, synthesis, and pharmacology, *J. Med. Chem.* 53 (2010) 6490–6505.
- [38] E. Dolusic, P. Larrieu, L. Moineaux, V. Stroobant, L. Pilote, D. Colau, L. Pochet, B. Van den Eynde, B. Masereel, J. Wouters, R. Frederick, Tryptophan 2, 3-dioxigenase (TDO) inhibitors, 3-(2-(Pyridyl) ethenyl) indoles as potential anticancer immunomodulators, *J. Med. Chem.* 54 (2011) 5320–5334.
- [39] S. Varshney, K. Shankar, M. Beg, V.M. Balaramnavar, S.K. Mishra, P. Jagdale, S. Srivastava, Y.S. Chhonker, V. Lakshmi, B.P. Chaudhari, R.S. Bhatta, A.K. Saxena, A.N. Gaikwad, Rohitukine inhibits in vitro adipogenesis arresting mitotic clonal expansion and improves dyslipidemia in vivo, *J. Lipid Res.* (2014), <http://dx.doi.org/10.1194/jlr.M039925>.
- [40] P. Prathipati, A. Dixit, A.K. Saxena, Computer-aided drug design: integration of structure-based and ligand-based approaches in drug design, *Curr. Comp. Aided Drug Des.* 3 (2007) 133–148.
- [41] G. Klebe, U. Abraham, T. Mietzner, Molecular similarity indices in a comparative analysis (CoMSIA) of drug molecules to correlate and predict their biological activity, *J. Med. Chem.* 37 (1994) 4130–4146.
- [42] G. Klebe, U. Abraham, Comparative molecular similarity index analysis (CoMSIA) to study hydrogen-bonding properties and to score combinatorial libraries, *J. Comput. Aided Mol. Des.* 13 (1999) 1–10.
- [43] Catalyst, Release Version 4.1, Accelrys Inc., San Diego, CA, 2006.
- [44] W. Sippel, Development of biologically active compounds by combining 3D QSAR and structure-based design methods, *J. Comput. Aided Mol. Des.* 16 (2002) 825–830.
- [45] R. Wang, Y. Lu, S. Wang, Comparative evaluation of 11 scoring functions for molecular docking, *J. Med. Chem.* 46 (2003) 2287–2303.
- [46] E.M. Krovat, T. Langer, Impact of scoring functions on enrichment in docking-based virtual screening: an application study on renin inhibitors, *J. Chem. Inf. Comput. Sci.* 44 (2004) 1123–1129.
- [47] M. Feher, Consensus scoring for protein–ligand interactions, *Drug Discov. Today* 11 (2006) 421–428.
- [48] C. Michaux, X. de Leval, F. Julemont, J.M. Dogne, B. Pirotte, F. Durant, Structure-based pharmacophore of COX-2 selective inhibitors and identification of original lead compounds from 3D database searching method, *Eur. J. Med. Chem.* 41 (2006) 1446–1455.
- [49] D. Schuster, E.M. Maurer, C. Laggner, L.G. Nashev, T. Wilckens, T. Langer, A. Odermatt, The discovery of new 11b-hydroxysteroid dehydrogenase type 1 inhibitors by common feature pharmacophore modeling and virtual screening, *J. Med. Chem.* 49 (2006) 3454–3466.
- [50] C. Laggner, C. Schieferer, B. Fiechtner, G. Poles, R.D. Hoffmann, H. Glossmann, T. Langer, F.F. Moebius, Discovery of high-affinity ligands of s1 receptor, ERG2, and enopamil binding protein by pharmacophore modeling and virtual screening, *J. Med. Chem.* 48 (2005) 4754–4764.
- [51] M.L. Lopez-Rodriguez, B. Benhamu, T. de la Fuente, A. Sanz, L. Pardo, M. Campillo, A three dimensional pharmacophore model for 5-Hydroxytryptamine 6 (5-HT6) receptor antagonists, *J. Med. Chem.* 48 (2005) 4216–4219.

- [52] O. Guner, O. Clement, Y. Kurogi, Pharmacophore modeling and three dimensional database searching for drug design using catalyst: recent advances, *Curr. Med. Chem.* 11 (2004) 2991–3005.
- [53] A. Kober, I. Sjöholm, The binding sites on human serum albumin for some nonsteroidal antiinflammatory drugs, *Mol. Pharmacol.* 18 (1980) 421–426.
- [54] U. Kragh-Hansen, Molecular aspects of ligand binding to serum albumin, *Pharmacol. Rev.* 33 (1981) 17–53.
- [55] K.J. Fehske, W.E. Müller, U. Wollert, The location of drug binding sites in human serum albumin, *Biochem. Pharmacol.* 30 (1981) 687–692.
- [56] R. Kun, L. Kis, I. Dekany, Hydrophobization of bovine serum albumin with cationic surfactants with different hydrophobic chain length, *Colloids Surf. B Biointerfaces* 79 (2010) 61–68.
- [57] B. Liu, Y. Guo, J. Wang, R. Xu, X. Wang, D. Wang, L. Zhang, Y. Xuc, Spectroscopic studies on the interaction and sonodynamic damage of neutral red (NR) to bovine serum albumin (BSA), *J. Lumin.* 130 (2010) 1036–1043.
- [58] G.H. Xiang, C.L. Tong, H.Z. Lin, Nitroaniline isomers interaction with bovine serum albumin and toxicological implications, *J. Fluoresc.* 17 (2007) 512–521.
- [59] E.L. Gelamo, M. Tabak, Spectroscopic studies on the interaction of bovine (BSA) and human (HSA) serum albumins with ionic surfactants, *Spectrochim. Acta A Mol. Biomol. Spectrosc.* 56A (2000) 2255–2271.
- [60] Y.A. Puius, Y. Zhao, M. Sullivan, D.S. Lawrence, S.C. Almo, Z.Y. Zhang, Identification of a second aryl phosphate-binding site in protein-tyrosine phosphatase 1B: a paradigm for inhibitor design, *Proc. Natl. Acad. Sci. U. S. A.* 94 (1997) 13420–13425.
- [61] C.P. Holmes, X. Li, Y. Pan, C. Xu, A. Bhandari, C.M. Moody, J.A. Miguel, S.W. Ferla, M.N. De Francisco, B.T. Frederick, S. Zhou, N. Macher, L. Jang, J.D. Irvine, J.R. Grove, PTP1B inhibitors: synthesis and evaluation of difluoromethylene phosphonate bioisosteres on a sulfonamide scaffold, *Bioorg. Med. Chem. Lett.* 18 (2008) 2719–2724.
- [62] C.P. Holmes, X. Li, Y. Pan, C. Xu, A. Bhandari, C.M. Moody, J.A. Miguel, S.W. Ferla, M.N. De Francisco, B.T. Frederick, S. Zhou, N. Macher, L. Jang, J.D. Irvine, J.R. Grove, Discovery and structure-activity relationships of novel sulfonamides as potent PTP1B inhibitors, *Bioorg. Med. Chem. Lett.* 15 (2005) 4336–4341.
- [63] J. Rao, R.C. Srimal, E. Audry, A. Carpy, A.K. Saxena, Synthesis and molecular lipophilicity potential profiles of 1-[*(3-methylphenyl)* piperazin-1-yl]-3-[thio(*4-acetamido*)phenyl]propane : a potential hypotensive agents, *Chem.-Inform* 22 (1991) 200.
- [64] M. Saxena, S.K. Agarwal, G.K. Patnaik, A.K. Saxena, Synthesis, biological evaluation and QSAR analysis of β -arylaminoethyl and β -arylpropionamidopiperazines/piperidines/-pyrazinopyridoindoles/pyrazinoisoquinolines. A new class of potent H1-antagonists, *J. Med. Chem.* 33 (1990) 2970–2976.
- [65] A.K. Saxena, M. Saxena, H. Chi, M. Wiese, Identification of a pharmacophore by application of hypothetical active site lattice (HASL) approach, *Med. Chem. Res.* 3 (1993) 201–208.
- [66] V.M. Balaramnavar, I.A. Khan, J.A. Siddiqui, M.P. Khan, B. Chakravarti, K. Sharan, G. Swarnkar, N. Rastogi, H.H. Siddiqui, D.P. Mishra, N. Chattopadhyay, A.K. Saxena, Identification of novel 2-((1-(benzyl(2-hydroxy-2-phenylethyl) amino)-1-oxo-3-phenylpropan-2-yl)carbamoyl)benzoic acid analogues as BMP-2 stimulators, *J. Med. Chem.* 55 (2012) 8248–8259.
- [67] S. Sharma, A.K. Pandey, P.K. Shukla, A.K. Saxena, Synthesis and 2D QSAR of O-sulphonated β -aminols derivatives as novel antifungal and antibacterial agents, *Bioorg. Med. Chem. Lett.* 21 (2011) 6476–6481.
- [68] R. Srivastava, S.P. Srivastava, N. Jaiswal, A. Mishra, R. Maurya, A.K. Srivastava, Antidiabetic and antidilipidemic activities of *C. cynamum* L. in validated animal models, *Med. Chem. Res.* 20 (2011) 1656–1666.
- [69] S. Dadke, J. Kusari, J. Chernoff, Down-regulation of insulin signaling by protein-tyrosine phosphatase 1B is mediated by an N-terminal binding region, *J. Biol. Chem.* 275 (2000) 23642–23647.
- [70] M. Kasuga, Y. Fujita-Yamaguchi, D.L. Blithe, C.R. Kahn, Tyrosine-specific protein kinase activity is associated with the purified insulin receptor, *Proc. Natl. Acad. Sci. U. S. A.* 80 (1983) 2137–2141.
- [71] A.D. Kohn, S.A. Summers, M.J. Birnbaum, R.A. Roth, Expression of a constitutively active Akt/Ser/Thr kinase in 3T3-L1 adipocytes stimulates glucose uptake and glucose transporter 4 translocation, *J. Biol. Chem.* 271 (1996) 31372–31378.
- [72] E. Hajduch, F. Darakhshan, H.S. Hundal, Fructose uptake in rat adipocytes: glut5 expression and the effects of streptozotocin-induced diabetes, *Diabetologia* 41 (1998) 821–828.
- [73] J. Zdychová, R. Komers, Emerging role of Akt kinase/protein kinase B signaling in pathophysiology of diabetes and its complications, *Physiol. Res.* 54 (2005) 1–16.
- [74] N.B. Ruderman, D. Carling, M. Prentki, J.M. Cacicedo, AMPK, insulin resistance, and the metabolic syndrome, *J. Clin. Invest.* 123 (2013) 2764–2772.
- [75] B.B. Zhang, G. Zhou, C. Li, AMPK: an emerging drug target for diabetes and the metabolic syndrome, *Cell Metab.* 5 (2009) 407–416.
- [76] L. Chen, Z. Jia, G. Yang, PPARs and metabolic syndrome. *PPAR Res.* <http://dx.doi.org/10.1155/2014/832606>.
- [77] R.M. Evans, G.D. Barish, Y.X. Wang, PPARs and the complex journey to obesity, *Nat. Med.* 4 (2004) 355–361.
- [78] Z.K. Wan, J. Lee, W. Xu, D.V. Erbe, D. Joseph-McCarthy, B.C. Follows, Y.L. Zhang, Monocyclic thiophenes as protein tyrosine phosphatase1B inhibitors: capturing interactions with Asp48, *Bioorg. Med. Chem. Lett.* 16 (2006) 4941–4945.
- [79] A.F. Moretto, S.J. Kirincich, W.X. Xu, M.J. Smith, Z.K. Wan, D.P. Wilson, B.C. Follows, E. Binnun, D. Joseph-McCarthy, K. Foreman, D.V. Erbe, Y.L. Zhang, S.K. Tam, S.Y. Tama, J. Leea, Bicyclic and tricyclic thiophenes as protein tyrosine phosphatase 1B inhibitors, *Bioorg. Med. Chem.* 14 (2006) 2162–2177.
- [80] D.P. Wilson, Z.K. Wan, W.X. Xu, S.J. Kirincich, B.C. Follows, D. Joseph-McCarthy, K. Foreman, A. Moretto, J. Wu, M. Zhu, E. Binnun, Y.L. Zhang, M. Tam, D.V. Erbe, J. Tobin, X. Xu, L. Leung, A. Shilling, S.Y. Tam, T.S. Mansour, J. Lee, Structure-based optimization of protein tyrosine phosphatase 1B inhibitors: from the active site to the second phosphotyrosine binding site, *J. Med. Chem.* 50 (2007) 4681–4698.
- [81] Z.K. Wan, B. Follows, S. Kirincich, D. Wilson, E. Binnun, W. Xu, D. Joseph-McCarthy, J. Wu, M. Smith, Y.L. Zhang, M. Tam, D. Erbe, S. Tam, E. Saiah, J. Lee, Probing acid replacement of thiophene PTP1B inhibitors, *Bioorg. Med. Chem.* 17 (2007) 2913–2920.
- [82] R. Thomsen, M.H. Christensen, MolDock: a new technique for high-accuracy molecular docking, *J. Med. Chem.* 49 (2006) 3315–3321.
- [83] G. Jones, P. Willett, R.C. Glen, A.R. Leach, R. Taylor, Development and validation of a genetic algorithm for flexible docking, *J. Mol. Biol.* 267 (1997) 727–748.